

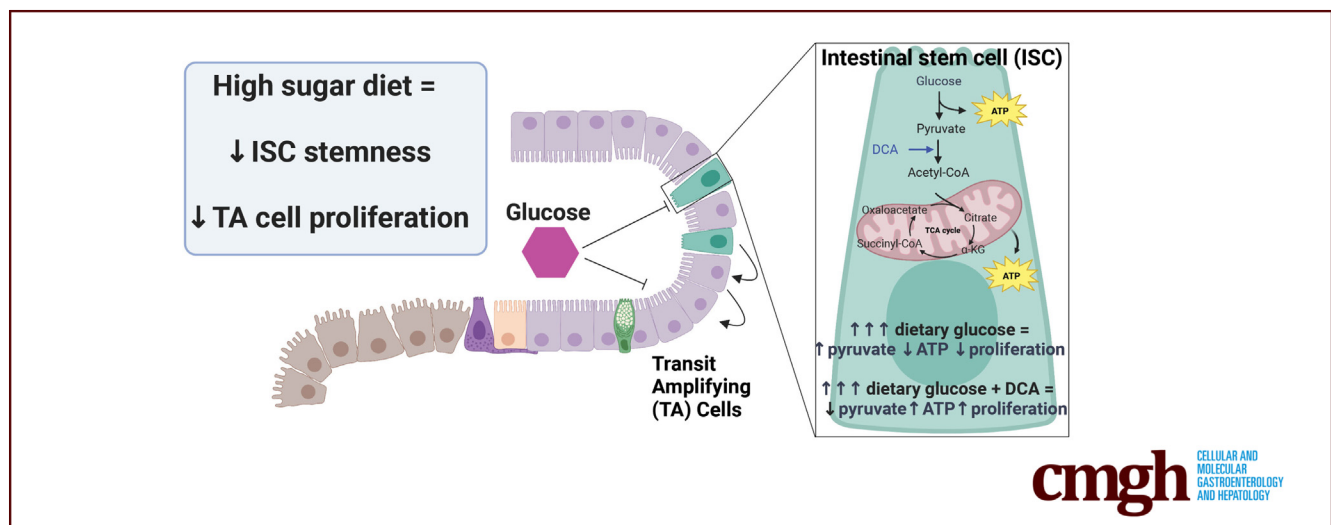
## ORIGINAL RESEARCH

## Excess Dietary Sugar Alters Colonocyte Metabolism and Impairs the Proliferative Response to Damage



Ansen H. P. Burr,<sup>1,2</sup> Junyi Ji,<sup>3</sup> Kadir Ozler,<sup>4</sup> Heather L. Mentrup,<sup>5</sup> Onur Eskiocak,<sup>4</sup> Brian Yueh,<sup>4</sup> Rachel Cumberland,<sup>6</sup> Ashley V. Menk,<sup>6</sup> Natalie Rittenhouse,<sup>1</sup> Chris W. Marshall,<sup>7</sup> Pailin Chiaranunt,<sup>1</sup> Xiaoyi Zhang,<sup>1,8</sup> Lauren Mullinax,<sup>1,8</sup> Abigail Overacre-Delgoffe,<sup>1</sup> Vaughn S. Cooper,<sup>7</sup> Amanda C. Poholek,<sup>1,2</sup> Greg M. Delgoffe,<sup>2,6</sup> Kevin P. Mollen,<sup>5</sup> Semir Beyaz,<sup>4</sup> and Timothy W. Hand<sup>1,2</sup>

<sup>1</sup>Richard King Mellon Institute for Pediatric Research, Pediatrics Department, Infectious Disease Section, University of Pittsburgh Medical Center Children's Hospital of Pittsburgh, University of Pittsburgh, Pittsburgh, Pennsylvania; <sup>2</sup>Department of Immunology, University of Pittsburgh, School of Medicine, Pittsburgh, Pennsylvania; <sup>3</sup>School of Medicine, Tsinghua University, Beijing, China; <sup>4</sup>Cold Spring Harbor Laboratory, Cold Spring Harbor, New York; <sup>5</sup>Department of Surgery, University of Pittsburgh School of Medicine, University of Pittsburgh Medical Center Children's Hospital of Pittsburgh, Pittsburgh, Pennsylvania; <sup>6</sup>Tumor Microenvironment Center, University of Pittsburgh Medical Center Hillman Cancer Center, Pittsburgh, Pennsylvania; <sup>7</sup>Department of Microbiology and Molecular Genetics, University of Pittsburgh, School of Medicine, Pittsburgh, Pennsylvania; and <sup>8</sup>Department of Gastroenterology, University of Pittsburgh School of Medicine, University of Pittsburgh Medical Center Children's Hospital



## SUMMARY

Excess sugar in the diet directly modifies the metabolism and transcriptome of the colonic epithelium. Sugar-mediated effects on colonic stem and transit-amplifying cells reduces their proliferative ability and inhibits their restorative capability after damage.

**BACKGROUND & AIMS:** The colonic epithelium requires continuous renewal by crypt resident intestinal stem cells (ISCs) and transit-amplifying (TA) cells to maintain barrier integrity, especially after inflammatory damage. The diet of high-income countries contains increasing amounts of sugar, such as sucrose. ISCs and TA cells are sensitive to dietary metabolites, but whether excess sugar affects their function directly is unknown.

**METHODS:** Here, we used a combination of 3-dimensional colonoids and a mouse model of colon damage/repair (dextran sodium sulfate colitis) to show the direct effect of sugar on the transcriptional, metabolic, and regenerative functions of crypt ISCs and TA cells.

**RESULTS:** We show that high-sugar conditions directly limit murine and human colonoid development, which is associated with a reduction in the expression of proliferative genes, adenosine triphosphate levels, and the accumulation of pyruvate. Treatment of colonoids with dichloroacetate, which forces pyruvate into the tricarboxylic acid cycle, restored their growth. In concert, dextran sodium sulfate treatment of mice fed a high-sugar diet led to massive irreparable damage that was independent of the colonic microbiota and its metabolites. Analyses on crypt cells from high-sucrose-fed mice showed a reduction in the expression of ISC genes, impeded proliferative potential, and increased glycolytic potential without a commensurate increase in aerobic respiration.

**CONCLUSIONS:** Taken together, our results indicate that short-term, excess dietary sucrose can directly modulate intestinal crypt cell metabolism and inhibit ISC/TA cell regenerative proliferation. This knowledge may inform diets that better support the treatment of acute intestinal injury. (*Cell Mol Gastroenterol Hepatol* 2023;16:287–316; <https://doi.org/10.1016/j.jcmgh.2023.05.001>)

**Keywords:** Stemness; Renewal; DCA; Mitochondria; Colitis.

The intestinal barrier is exposed to billions of microorganisms, dietary products, and metabolites every day. To prevent barrier failure and bacteremia, the intestinal epithelium is replaced every 3–5 days by leucine rich repeat containing G protein-coupled receptor 5 positive (*Lgr5*<sup>+</sup>) intestinal stem cells (ISCs).<sup>1</sup> ISCs reside at the base of crypts and asymmetrically divide to self-renew and to generate transit-amplifying (TA) cells, which rapidly divide as they move up crypts and differentiate into mature epithelial subsets such as goblet cells, enteroendocrine cells, and absorptive enterocytes.<sup>2,3</sup> After intestinal damage, rapid proliferation of crypts is particularly important to replace lost and damaged cells.<sup>4</sup>

Diet-derived metabolites directly alter both the proliferation and stemness of ISCs. For example, a high-fat diet increases both the self-renewal and proliferative capacity of ISCs/TA cells owing to a metabolic preference for fatty acid oxidation and aerobic respiration.<sup>5,6</sup> The modern diet of high-income countries is characterized by increased consumption of dietary sugar, especially “acellular sugar,” that are absorbed by the host without additional digestion.<sup>7–9</sup> Indeed, the rate of sugar consumption has increased by 127% in the past 40 years<sup>10</sup>; how these dietary changes affect intestinal health is still unclear. Elucidating how diet affects ISC function will have important implications for understanding how the intestinal epithelium is restored after damage caused by infection, inflammatory bowel diseases (IBDs), or radiation therapy.

Here, we show high-sugar concentrations directly impair the development of organoids grown from mouse or human colons and increase the glycolytic metabolite pyruvate, while decreasing cellular energy levels (adenosine triphosphate [ATP]). Treatment with dichloroacetate (DCA) increased pyruvate entry into the tricarboxylic acid (TCA) cycle and restored the metabolite profile, transcriptome, and proliferative ability of colonoids grown under high-sugar concentrations. Mice fed a high-sucrose diet while undergoing dextran sodium sulfate (DSS) treatment develop lethal barrier failure as a result of impaired colonocyte proliferation within 6 days and these results were recapitulated in germ-free mice, which shows that this effect is independent of the microbiota. Metabolic analysis of colonic crypts isolated from mice fed a high-sucrose (HS) diet showed increased glycolytic potential without a requisite increase in aerobic respiration. Transcriptome and imaging data confirmed HS-fed mice have reduced expression of proliferative genes in ISCs and TAs and this phenotype is exacerbated by DSS-induced

damage. Together, these studies elucidate the damaging effects HS can have on the regenerative capacity of colonic epithelium during acute injury.

## Results


### High-Sugar Conditions Impair 3-Dimensional Colonoid Development

To determine the direct effect of media sugar concentrations on the development of mature colonocytes, we used 3-dimensional epithelial colonoids generated from colonic crypts. Increasing the concentration of glucose, fructose, or sucrose led to a dose-dependent reduction in murine colonoid growth as measured by viability, number, and size (Figure 1A and B). Human colonoids also showed inhibited growth into colonoid structures when exposed to high-sugar concentrations (Figure 1C and D). RNA sequencing (RNA-seq) analysis of murine colonoids revealed that high-glucose concentrations (additional 150 mmol/L) significantly reduced expression of core ISC genes such as *Lgr5*, *Tnfrsf19*, and *Rgcc* (Figure 1E). Furthermore, gene set enrichment analysis (GSEA) showed enrichment in control-treated colonoids for gene sets associated with E2F transcription factor targets and the ISC gene signature (Figure 1F). Reduced colonoid growth was not caused by osmotic stress because fully developed mouse and human colonoids were viable when cultured for 48 hours in up to 400 mmol/L added sucrose, fructose, or glucose (Figure 2). Therefore, our data suggest that high-sugar conditions impair ISC function and proliferation, leading to direct inhibition of murine and human colonoid development in vitro.

### High-Glucose Conditions Reduce Pyruvate Flux Into the TCA Cycle

Cellular metabolism is important for proliferation and metabolite availability can regulate cell-cycle progression.<sup>11</sup> For example, fatty acid oxidation is required for ISC survival and epithelial renewal, and increasing access to fatty acids increases the tumorigenicity of ISCs.<sup>5,12–14</sup> We

**Abbreviations used in this paper:** ATP, adenosine triphosphate; BSA, bovine serum albumin; DMEM, Dulbecco's modified Eagle medium; DSS, dextran sodium sulfate; ECAR, extracellular acidification rate; EdU, 5-ethynyl-2'-deoxyuridine; EGF, epidermal growth factor; EPCAM, epithelial cellular adhesion molecule; FCCP, carbonyl cyanide p-trifluoromethoxyphenylhydrazone; FITC, fluorescein isothiocyanate; FMT, fecal microbiome transfer; GSEA, gene set enrichment analysis; HF, high-fiber; HS, high-sugar; IBD, inflammatory bowel disease; ISC, intestinal stem cell; *Lgr5*, leucine rich repeat containing G protein-coupled receptor 5; OCR, oxygen consumption rate; PBS, phosphate-buffered saline; PDH, pyruvate dehydrogenase; PDHK, pyruvate dehydrogenase kinase; p-PDH, phosphorylated-PDH; RNAseq, RNA sequencing; ROS, reactive oxygen species; rRNA, ribosomal RNA; SCFA, short-chain fatty acid; SRC, spare respiratory capacity; Std, standard; TA, transit-amplifying; TCA, tricarboxylic acid; TUNEL, terminal deoxynucleotidyl transferase-mediated deoxyuridine triphosphate nick-end labeling.

 Most current article

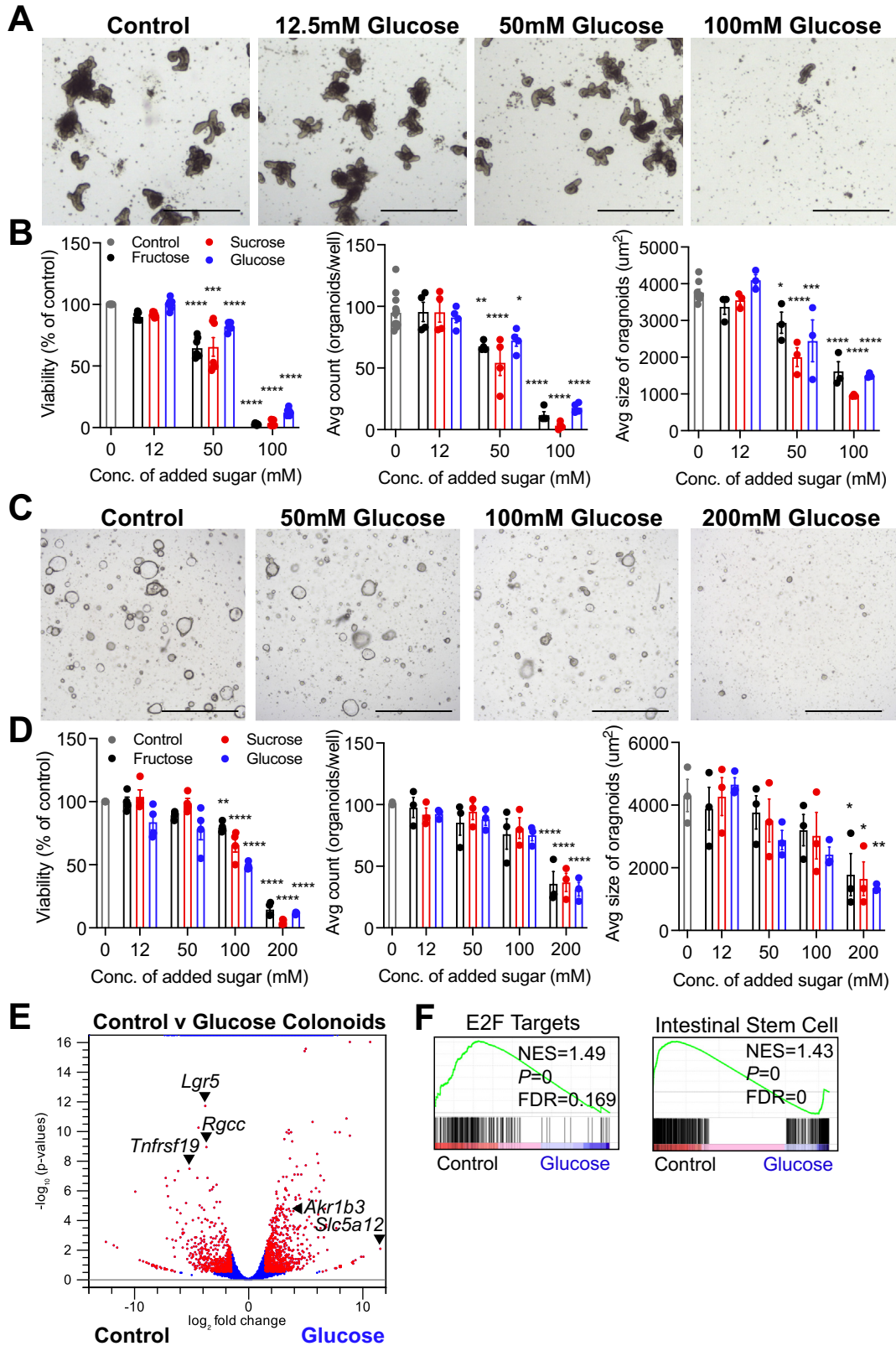
© 2023 The Authors. Published by Elsevier Inc. on behalf of the AGA Institute. This is an open access article under the CC BY-NC-ND license (<http://creativecommons.org/licenses/by-nc-nd/4.0/>).

2352-345X

<https://doi.org/10.1016/j.jcmgh.2023.05.001>

compared the metabolite composition of colonoids cultured in high (100 mmol/L) or low (25 mmol/L) added glucose concentrations for 4 days so that we could capture the effects

of chronically increased sugar on metabolism. We found that under high-glucose conditions, colonoids had decreased levels of ATP and increased levels of adenosine diphosphate



and adenosine monophosphate (Figure 3A–E), which strongly suggests reduced efficiency of cellular metabolism. Accordingly, we observed reduced levels of key glycolysis-associated metabolites that are downstream of enzymatic reactions that require ATP hydrolysis, such as fructose-1/2,6-bisphosphate, 3-phosphoglycerate, and phosphoenolpyruvate in high-glucose conditions (Figure 3A and F–H). Conversely, high-glucose conditions increased pyruvate, suggesting a buildup of the final metabolite in the glycolysis pathway (Figure 3J). TCA cycle metabolites were largely unaffected or slightly increased by high-glucose conditions (Figure 4A–H), suggesting colonoids are passing glycolytic metabolites into the TCA cycle. However, the buildup of pyruvate and reduction in ATP imply that the transfer of this metabolite to the TCA cycle may be affected negatively. High-glucose conditions did not alter extracellular lactate levels, suggesting high-glucose-treated colonoids are not shunting pyruvate to lactate (Figure 4I). Pyruvate also can be used as a substrate for the anabolism of alanine, glycine, and serine, and high-glucose conditions induced increases in all 3 of these amino acids (Figure 3J–L), suggesting this may be a compensatory sink for accumulated intracellular pyruvate. Finally, we found that high-glucose conditions led to the accumulation of metabolites associated with palmitate oxidation such as carnitine and carnitine-derived fatty acids (Figure 3M–O), suggesting impaired fatty acid breakdown for oxidative fuel metabolism. These results indicate that in colonoids, high-glucose conditions substantially modify cellular metabolism, increasing the accumulation of pyruvate and decreasing energy (ATP) production.

### Coupling Glycolysis With Aerobic Respiration Restores Sugar-Impaired Colonoid Development and Metabolic Efficiency

Phosphorylation of pyruvate dehydrogenase (PDH) by pyruvate dehydrogenase kinase (PDHK) inactivates PDH and blocks the flux of glycolytic metabolites into the TCA cycle. Typically, high levels of pyruvate inhibit PDHK, which leads to the disinhibition of PDH and increased conversion of pyruvate to acetyl-CoA.<sup>15</sup> However, even though glucose-treated colonoids have high levels of pyruvate, phosphorylated-PDH (p-PDH) levels were similar between glucose and control-treated colonoids, suggesting dysregulation of pyruvate metabolism (Figure 4J). To determine whether

blocking PDHK could restore colonoid growth, we treated isolated ISCs with the PDHK inhibitor DCA.<sup>16</sup> DCA significantly increased colonoid numbers developing from ISCs cultured in inhibitory levels (150 mmol/L) of sucrose, fructose, and added glucose, modestly restored pyruvate and related metabolites, and restored cellular energy (ATP) (Figures 3A–E and 5A and B). In contrast, no growth improvement was observed with rotenone, an inhibitor of the mitochondrial respiratory chain, or 2-deoxyglucose, a glycolysis inhibitor (Figure 5C). In accord with the restoration of colonoid growth, RNAseq analysis of colonoids treated with glucose/DCA showed increased expression of core ISC genes such as *Lgr5*, *Axin2*, and *Ascl2*, and GSEA revealed enrichment for gene sets associated with ISC signature in glucose/DCA-treated colonoids (compared with HS) (Figure 5D–G).

### Colonocytes Can Uptake Luminal Glucose In Vivo

Generally, the colon reabsorbs water and electrolytes while the small intestine uptakes nutrients. To determine whether dietary glucose can be absorbed directly by colonocytes in vivo, we introduced fluorescently labeled glucose (Cy5-linked 1-amino-glucose)<sup>17,18</sup> via enema into *Lgr5* reporter mice (*Lgr5*<sup>eGFP-cre-ERT2</sup>).<sup>1</sup> This glucose tracer was synthesized by direct amide coupling of cyan fluorophores to 1-amino-1-deoxy-D-glucose and bypassed the transporter-specificity issues of other fluorescent glucose analogs.<sup>17,19</sup> Importantly, we observed glucose uptake by *Lgr5*<sup>+</sup> ISCs, suggesting colonocytes can directly uptake luminal glucose (Figure 6A and B). Colonocytes express transporter genes that bring glucose into the cell from the lumen (*Slc5a1*; SGLT1) and glucose/fructose from the blood (*Slc2a1,3-6*; GLUT1, 3-6), but not GLUT2 (*Slc2a2*), the bidirectional transporter that exports glucose from small intestinal enterocytes into the blood<sup>20–22</sup> (Figure 6C). Thus, colonocytes do not export glucose by the canonical pathway and likely respond to high-sucrose conditions in a distinct manner compared with small intestinal epithelium. Excess sugar consumption has been linked to diabetes, and increased blood glucose impairs intestinal integrity.<sup>23</sup> However, when we increased the sugar content in experimental mouse diets, we detected no differences in fasted or postprandial blood glucose levels or in intestinal permeability of mice

**Figure 1. (See previous page). Excess sugar impairs colonoid growth and reduces the expression of genes associated with *Lgr5*<sup>+</sup> ISCs.** (A and B) Murine colonic crypts were cultured in increasing concentrations of sucrose, glucose, or fructose. (A) Representative images (magnification, 4×; scale bar: 200 μm), and (B) viability (percentage CellTiter-Glo luminescence of control), number, and size of colonoids after 5 days in culture are shown. (C and D) Human colonoids were dispersed to single cells and regrown with increasing concentrations of glucose. (C) Representative images (magnification, 4×; scale bar: 200 μm), and (D) average viability, number, and size of colonoids after 12 days in culture are shown. Data are representative of 2 experiments (n = 3) and data points are means ± SEM. One-way analysis of variance with multiple comparisons (with control), where \*P < .05, \*\*P < .01, \*\*\*P < .001, \*\*\*\*P < .0001. (E and F) Murine colonoids cultured in 25 mmol/L (control) or 150 mmol/L of added glucose (Glucose) for 5 days were analyzed via RNAseq. (E) Volcano plot comparing control vs glucose-treated colonoids, red points in the volcano plot represent differentially expressed genes (-1.5 > FC > 1.5; P < .05; FDR < 0.3). (F) GSEA showing enriched gene sets (control vs glucose-treated). Concentrations of sugar represent the amount added in addition to what is present in the media (25 mmol/L). Avg, average; Conc., concentration; FDR, False Discovery Rate; NES, Normalized Enrichment Score.

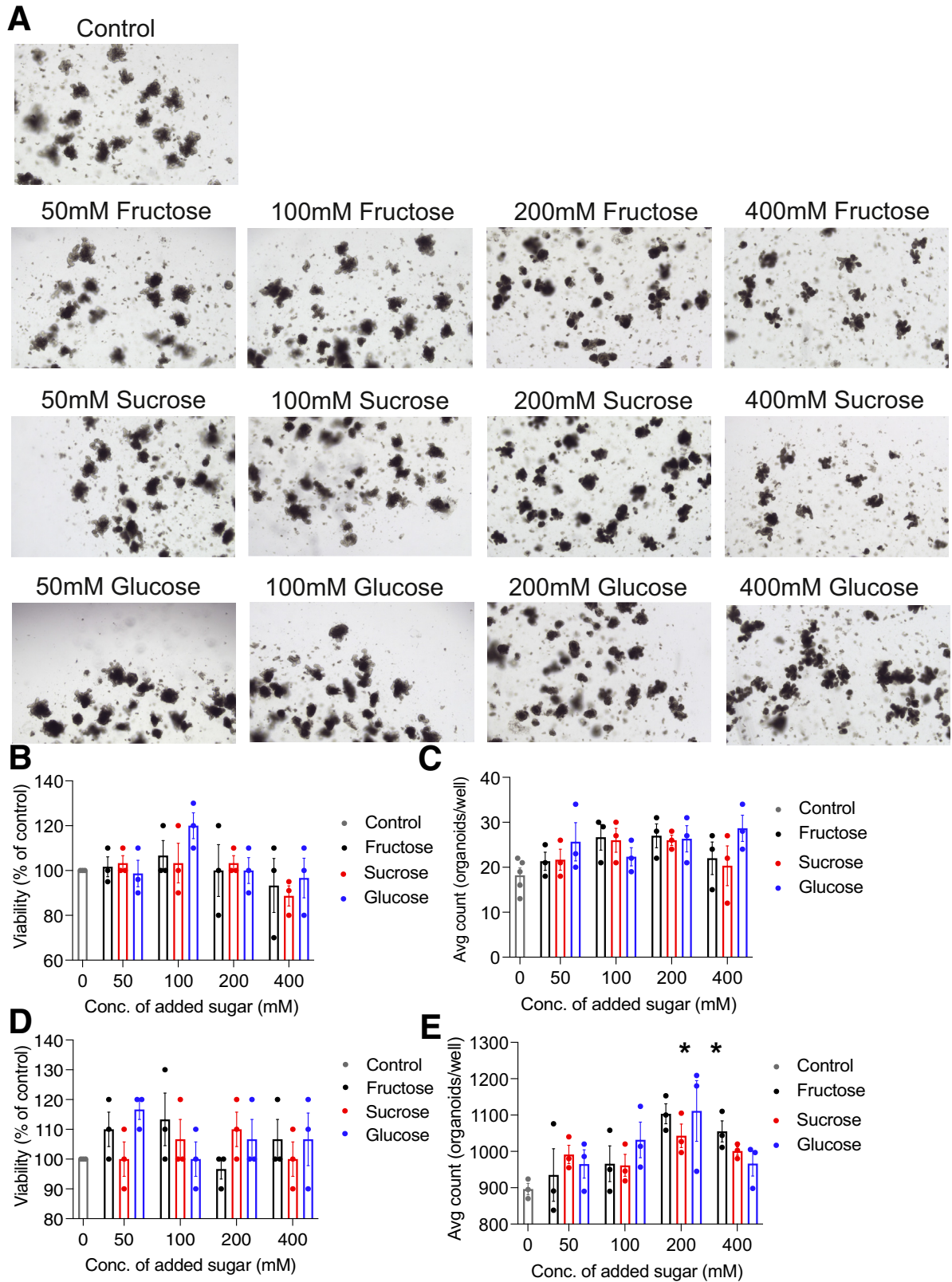


**Figure 2. Excess sugar is not toxic to fully developed colonoids.** (A–C) Colonic crypts were isolated from mice and cultured for 5 days into fully developed 3-dimensional colonoids, which then were exposed to increased concentrations of added sucrose, glucose, or fructose for 2 days. (A) Representative images, (B) viability (percentage CellTiter-Glo [CTG] luminescence of control), and (C) number of organoids per well are shown. Images were taken at a magnification of 4× (scale bars: 200 μm). (D and E) After developing into mature human colonoids for 5 days, excess sugar was added for 2 days. (D) Average viability (percentage CTG luminescence of control) and (E) number of human colonoids are shown. (B–E) Data are representative of 2 experiments (n = 3) and data points are means ± SEM. Statistics represent (B) Kruskal–Wallis or (C and D) 1-way analysis of variance with multiple comparisons with control. \**P* < .05. Avg, average; Conc., concentration.

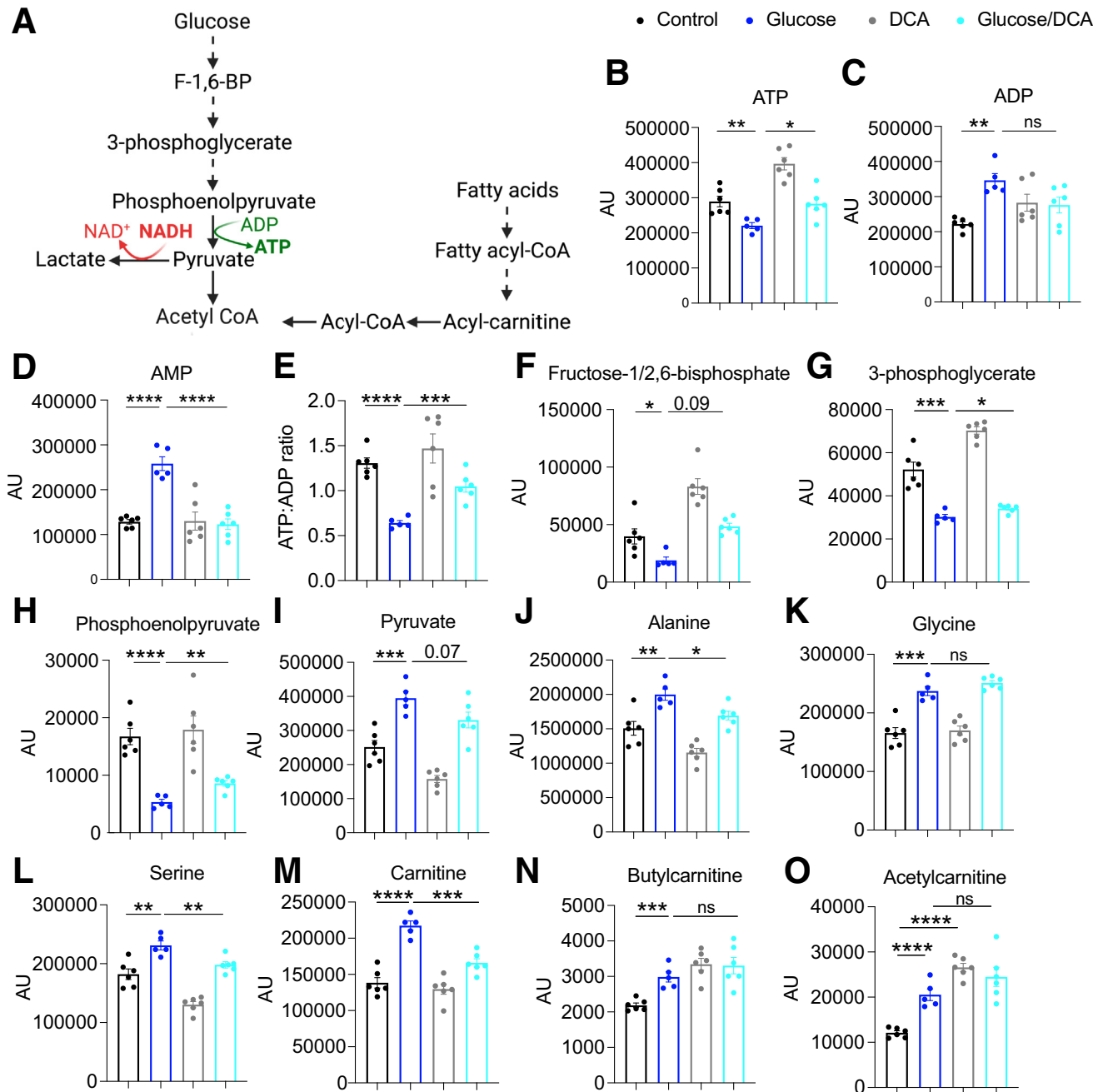


**Figure 3. Excess glucose increases intracellular pyruvate but reduces total ATP levels in colonoids, and both metabolites are restored with DCA treatment.** (A) Diagram of glycolysis and fatty acid oxidation pathways made with Biorender.com. (B–O) Isolated colonic crypts were cultured in 25 or 100 mmol/L of added glucose for 4 days, with and without 4 mmol/L DCA, and metabolite levels were measured via liquid chromatography–mass spectrometry. Quantified levels of metabolites as indicated. Data points represent means  $\pm$  SEM and are representative of 2 experiments ( $n = 3–6$ ). (C and F) Statistics represent 1-way analysis of variance or Kruskal–Wallis, where  $*P < .05$ ,  $**P < .01$ ,  $***P < .001$ ,  $****P < .0001$ . ADP, Adenosine di-phosphate; AMP, Adenosine mono-phosphate; AU, arbitrary units; BP, bisphosphonate; CoA, Coenzyme-A; NAD, Nicotinamide Adenine Dinucleotide; NADH, Nicotinamide Adenine Dinucleotide Hydride.

fed a HS diet compared with controls (Figure 6D–F). Taken together, our results support the concept that when consumed in high concentrations, luminal diet-derived sugar could be absorbed directly and affect colonic epithelial cells.

### HS Diet Leads to Lethal Colonic Damage When Exposed to DSS

To determine how increased dietary sucrose affects colonocyte repair in vivo, we treated mice with sugar-supplemented water and the chemical DSS as a murine

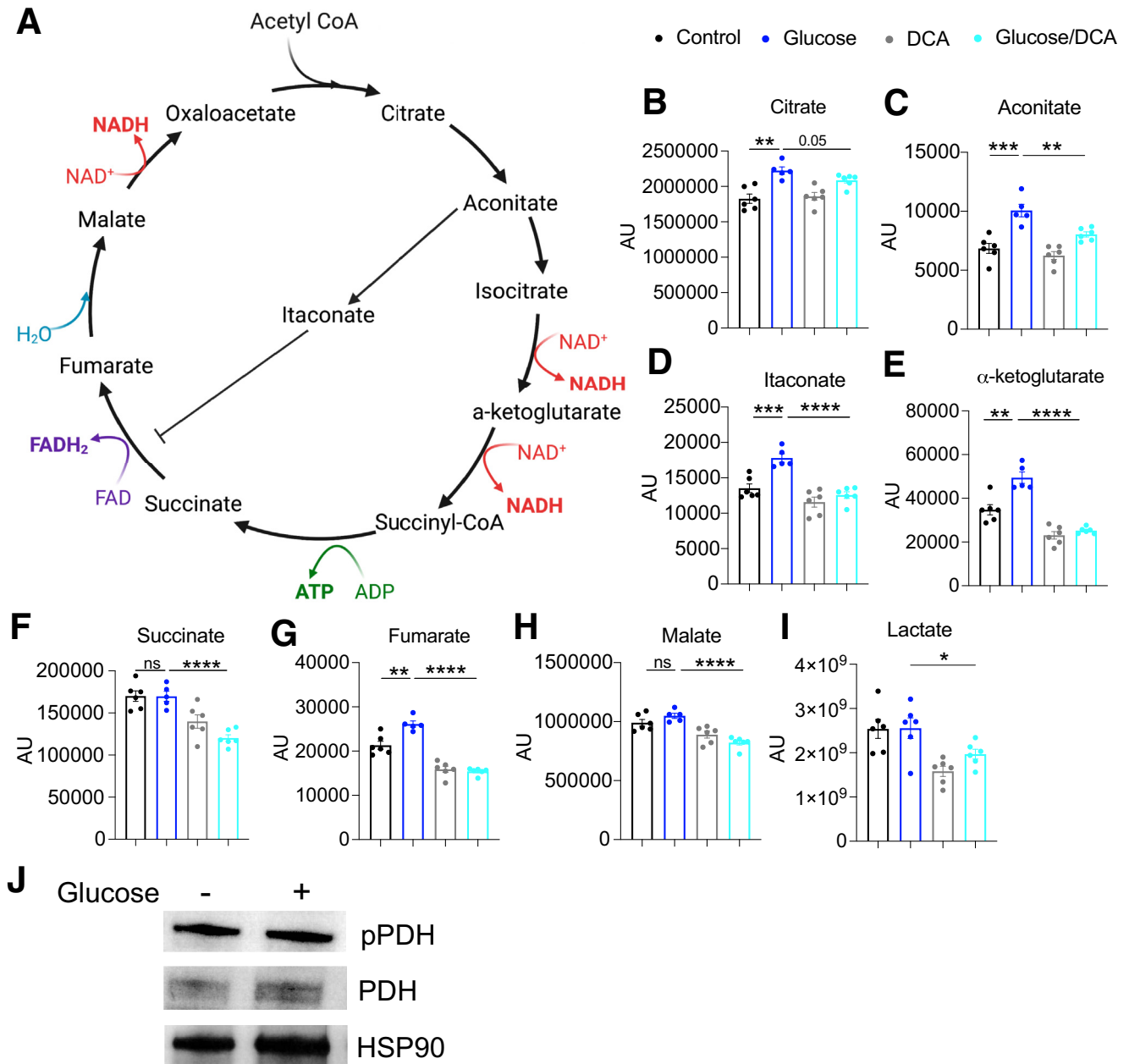


**Figure 4. Level of TCA cycle metabolites and phosphorylated PDH in glucose-treated colonoids.** (A) Schema of TCA cycle. (B–I) Colonoids were cultured from single cells in 25 or 100 mmol/L of added glucose (totaling 50 and 125 mmol/L, respectively) for 4 days and metabolite levels from (B) media or (C–I) cells were measured via liquid chromatography–mass spectrometry. Data points represent means  $\pm$  SEM and represent 2 experiments ( $n = 3$ –6). Statistics represent 1-way analysis of variance, where \* $P < .05$ , \*\* $P < .01$ , \*\*\* $P < .001$ , \*\*\*\* $P < .0001$ . (J) Colonoids were cultured from single cells with or without 100 mmol/L added glucose (totaling 25 mmol/L for the control and 125 mmol/L for glucose-treated) for 6 days and protein expression of phospho-PDH (pPDH), PDH, and heat shock protein (HSP)90 were measured via Western blot. Representative blot of 4 experiments is shown. ADP, Adenosine di-phosphate; AU, arbitrary units; CoA, Coenzyme-A; FAD, Flavin adenine dinucleotide; FADH<sub>2</sub>, Reduced Flavin adenine dinucleotide; HSP90, heat shock protein 90; NAD, Nicotinamide Adenine Dinucleotide; NADH, Nicotinamide Adenine Dinucleotide hydride.

model of intestinal damage. Sucrose is composed of 2 monosaccharides, glucose and fructose, which are differentially metabolized and absorbed in the intestine. We observed similar weight loss and lethal disease in 3% DSS-treated mice drinking water supplemented with fructose, glucose, or sucrose (all 10% by mass) (Figure 7A),

consistent with the impairment of colonoid growth by all 3 sugars. Glucose appeared to have the most severe effects (Figure 7A); however, all mice fed sweetened water died from DSS, while mice given unsweetened water lost less weight and recovered from colonic damage (Figure 7B). A potential confounder is that mice prefer sweetened water,<sup>24</sup>

which leads to increased DSS consumption (Figure 7C). Mice fed a HS diet consumed the same number of grams of sucrose per day as mice provided with 10% sucrose-supplemented drinking water (Figure 7D), while consuming the same amount of water as mice fed either a standard mouse diet (Std) (chow in facility similar in composition to the high-fiber [HF] diet) or the isocaloric HF diet (Figure 7C). Therefore, to control for DSS dosage, we focused on experiments that modify sucrose in the mouse chow. Switching to various defined carbohydrate diets (HF and HS) did not alter the weight of diet-treated mice significantly, the amount of food consumed, or the intestinal transit time (Figure 7E–I).

Compared with mice fed HF and Std, HS-fed mice had significantly greater weight loss and 100% mortality by day 9 of DSS treatment (Figure 8A and B). Histologic analysis showed that HS/DSS-treated mice showed massive immune infiltration and loss of crypt structure by day 6 of DSS (Figure 8C and D). This level of damage normally is seen approximately 9 days after DSS treatment,<sup>25</sup> suggesting that HS accelerates disease progression.

To determine the concentration of sucrose that is sufficient to induce the lethal DSS response, we reduced the percentage of sucrose incrementally in diets (Figure 8E). Diets that contained 20% or 5% of calories from sucrose did not induce the substantial early weight loss (day 6), but a dose-dependent response to sucrose clearly was observed starting at 35% sucrose (Figure 8E). Indeed, despite inducing more weight loss, 35% sucrose was not sufficient to induce the rapid death of higher sucrose concentrations, showing that there is a direct dose response to accelerated DSS damage and the amount of dietary sucrose (Figure 8F).

To test whether the effect of the HS diet is immediate or requires priming to accelerate lethal colonic disease, we fed mice Std or HS diets for 2 weeks and then reversed the diets on the first day of DSS treatment. Mice that were fed HS for 2 weeks and switched to a Std diet with the initiation of DSS lost weight similar to the group fed the Std diet throughout, while mice fed the Std diet and switched to the HS diet during DSS treatment lost weight similar to the group fed the HS diet throughout the experiment (Figure 8G and H). Therefore, excess sucrose must be present contemporaneously to exacerbate DSS-induced disease, but does not require more than 1 day of dietary priming before colonic damage to induce severe disease.

### Lethal DSS Colitis in HS-Fed Mice Is Independent of the Microbiome.

We hypothesized that sucrose may be altering the intestinal microbiota of HS-fed mice by expanding the population of *Enterobacteriaceae*, which thrive on simple carbohydrates.<sup>26,27</sup> Although 16S ribosomal RNA (rRNA) sequencing of fecal samples showed that defined diets altered the intestinal microbiota compared with Std-fed mice, there was no statistically significant difference between the microbiota of HS- or HF-fed mice as determined by principal coordinate, relative abundances, and Linear discriminant analysis Effect Size (LEfSe, Figure 9A–C and data not shown). Given that the

composition of HS and HF diets contrast only in carbohydrate source, these data show the importance of controlling for specific ingredients when comparing effects of diet on the microbiome. Seven days after DSS initiation, HS/DSS-treated mice showed an outgrowth of *Enterobacteriaceae* and *Enterococcaceae* (Figure 9B). However, these taxa expand under a variety of inflammatory intestinal conditions of varying severity, and are unlikely the sole cause of the rapid failure of the colonic epithelium seen in HS/DSS-treated mice.<sup>28</sup> Furthermore, Std-fed mice receiving sucrose-supplemented water died of DSS but did not show the same outgrowth of *Enterobacteriaceae* and *Enterococcaceae*, indicating that it is not necessary for lethal colitis (Figure 9B).

Both a fiber-free diet and sucrose-supplemented water contribute to the expansion of mucus-degrading bacteria, such as *Akkermansia* species, and increased susceptibility to colonic bacterial infection.<sup>29,30</sup> However, despite our HS diet containing low levels of fiber, the frequency of *Akkermansia* species did not discriminate HS- or HF-fed mice and thus cannot explain the phenotype of HS/DSS-treated mice (Figure 9D). Short-chain fatty acids (SCFAs) are microbiome-derived byproducts of dietary fiber that the host absorbs to provide nutrients to colonocytes, support the expansion of regulatory T cells, and dampen inflammation derived from innate immune cells.<sup>31–33</sup> The lower amount of fiber in the HS diet may result in decreased SCFAs to the host and possibly contribute to pathology. However, supplementing SCFAs in the water of HS-fed mice did not prevent lethal colitis (Figure 9E and F). To ensure that SCFA reached the colon, rather than being absorbed entirely by the small intestine, we also supplemented the HS diet with tributyrin, which is broken down into butyrate and absorbed in the colon.<sup>31,34</sup> Tributyrin supplementation did not rescue HS-fed mice, showing the same weight loss and lethality (Figure 9E and F), suggesting that it is not the relative lack of fiber and SCFA byproducts that is detrimental to colonic health during intestinal damage in our model, but excess sucrose.

We next tested whether HS diet directly can affect colonic regeneration in the absence of the microbiome by treating germ-free mice with a HS or Std diet and 1% DSS for 1 week. The HS diet resulted in accelerated lethal DSS colitis, with significantly greater weight loss and mortality than mice fed the Std diet (Figure 10A and B). Thus, the HS diet alone was sufficient to induce accelerated disease independent of the microbiome, showing a clear direct effect of the HS diet on epithelial response to damage in vivo.

To directly test whether functional shifts in the microbiome of HS-fed mice can worsen DSS colitis, we transferred fecal microbiome from HS- and HF-fed mice into germ-free, Std-fed mice, and treated with 3% DSS. Mice receiving HS microbiota (HS-fecal microbiome transfer [FMT]) showed decreased survival compared with germ-free mice that received HF microbiota (HF-FMT) (Figure 10C–E). However, mice that received HS-FMT did not lose weight as quickly as HS-fed mice, and they did not die in the first week of treatment, suggesting that although the microbiota contributes to the severity of DSS colitis in this model, it is not sufficient to induce the acute negative effects of excess dietary sucrose.



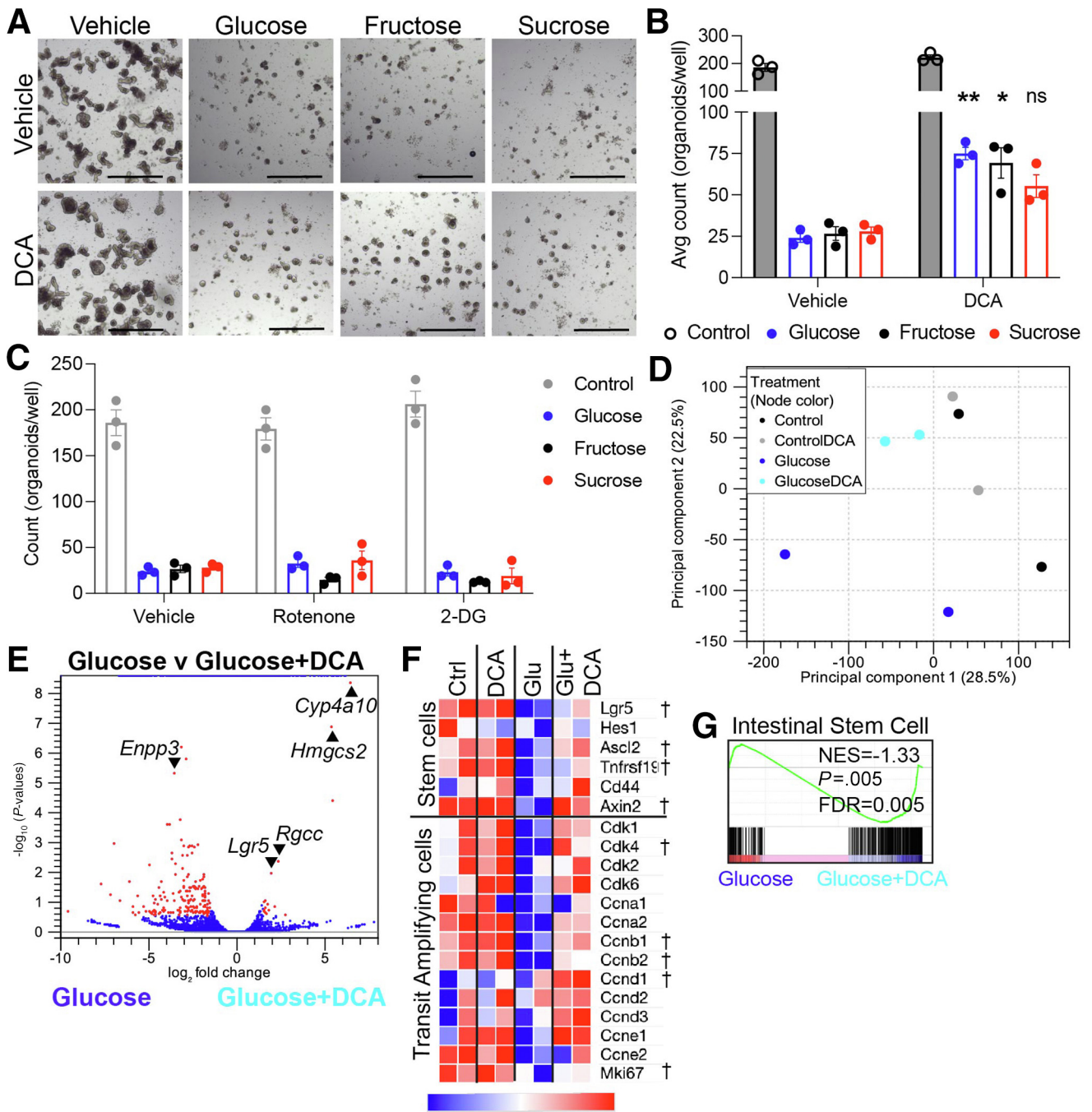


**Figure 5. Pyruvate dehydrogenase kinase inhibition with DCA rescues sugar-impaired colonoid development.** (A and B) Murine colonoids were cultured in 150 mmol/L added sucrose, fructose, glucose (totaling 175 mmol/L), or no-sugar-added control, with or without DCA (dichloroacetate, 4 mmol/L). (A) Representative images after 4 days of culture in sugar and metabolic inhibitors (magnification, 4×; scale bars: 200 μm). (B) Quantification of panel A. Statistics represent Mann-Whitney comparing vehicle with DCA-treated, where \**P* < .05, \*\**P* < .01. (C) Colonoids grown from single cells in 150 mmol/L of added sucrose, fructose, or glucose (totaling 175 mmol/L) for 4 days with or without 7.8 mmol/L rotenone or 1 mmol/L 2-deoxyglucose (2-DG) for 4 days. Number of colonoids is shown. Data points represent means ± SEM and represent 2 experiments (n = 3). Stats represent 2-way analysis of variance with multiple comparisons (with vehicle control). (D–G) Colonoids with and without added glucose and/or DCA treatment were analyzed by RNAseq. (D) Principal component analysis (PCA) plot and (E) volcano plot comparing the transcriptome of glucose- and glucose/DCA-treated colonoids. (F) Transcript expression level of characteristic epithelial subset genes from various treated colonoids, as indicated. (G) GSEA of ISC signature enrichment (glucose/DCA-treated vs glucose-treated). Red points in volcano plot and dagger in heatmap represent differentially expressed genes (-1.5 > FC > 1.5; *P* < .05; FDR < 0.3). Avg, average; Ctrl, control; FDR, False Discovery Rate; NES, Normalized Enrichment Score.

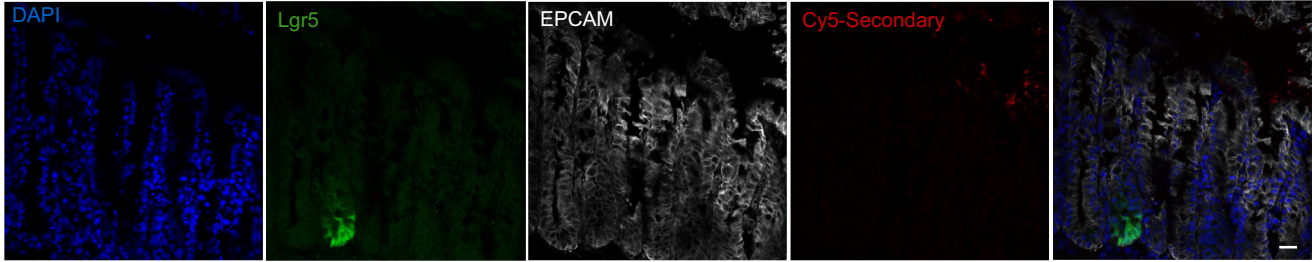
**Excess Dietary Sucrose Alters Colonic Crypt Metabolism, Increasing Spare Respiratory Capacity and Glycolytic Response**

To test whether the HS diet perturbs the metabolism of the colonic epithelium of mice, we isolated colonic crypts

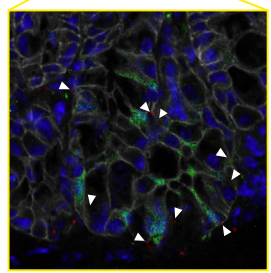
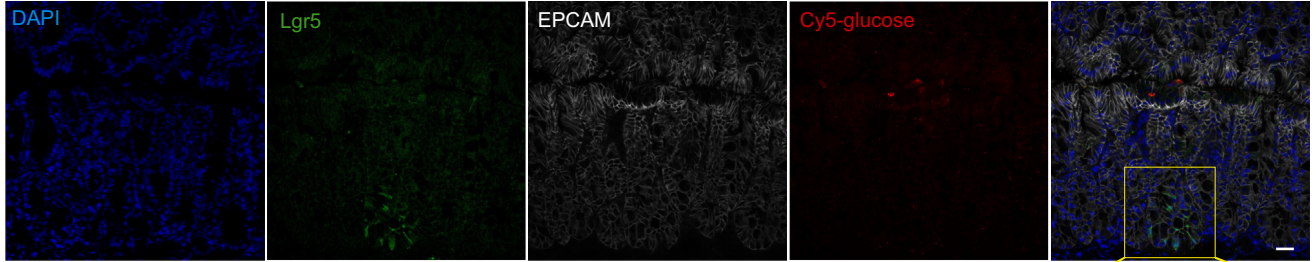
from mice fed a HS or HF diet for 2 weeks and analyzed their glycolytic and respiratory rates.<sup>6</sup> Colonic crypts from HS- and HF-fed mice did not differ in their basal aerobic respiration (oxygen consumption rate [OCR]) and basal anaerobic respiration (extracellular acidification rate

**A**

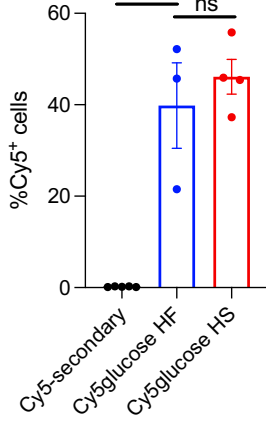
*Lgr5<sup>Cre</sup>* with Cy5-secondary enema control



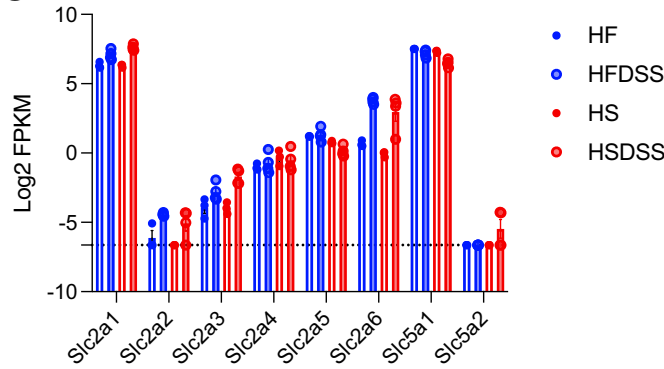
*Lgr5<sup>Cre</sup>* with Cy5-glucose enema



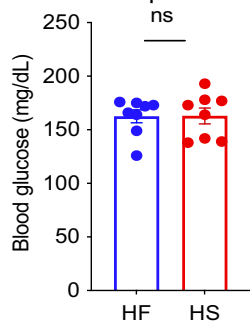
**B**



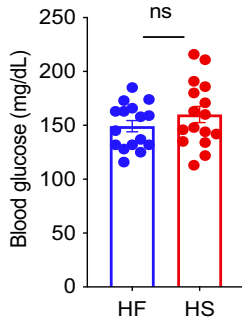
**C**



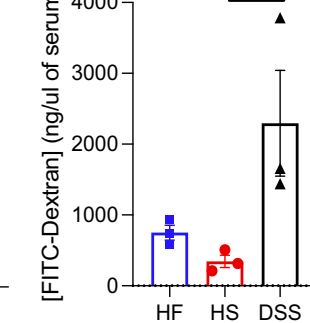
**D**



**E**



**F**



[ECAR]] (Figure 11A–D). As expected, colonic crypts displayed a high level of aerobic respiration, as shown by a high OCR:ECAR ratio (Figure 11E). In contrast, HS conditions increased the difference between basal and maximal oxidative rates, termed *spare respiratory capacity* (SRC) (as determined by uncoupling ATP synthesis from the electron transport chain with carbonyl cyanide p-trifluoromethoxyphenylhydrazone [FCCP] to maximize oxygen consumption) (Figure 11F and G). High SRC indicates mitochondrial potential that is not being used for basal ATP production and that can supply sudden bursts of energy.<sup>35</sup> However, proliferative cells and stem cells generally have low levels of SRC, indicating they largely use basal OCR to provide ATP, and increased SRC typically is associated with differentiated cells.<sup>36,37</sup> Interestingly, crypts from HS-fed mice still performed glycolysis after 3 hours of glucose deprivation, suggesting high-sucrose conditions may create a carbohydrate reservoir in colonocytes (Figure 11H and I). Oligomycin blocks the production of ATP from aerobic respiration, which should increase glycolysis, but neither crypts from HS- nor HF-fed mice showed a compensatory increase in glycolysis upon inhibition of respiration (Figure 11C and H).<sup>38</sup> HS-fed crypts have greater ATP-linked OCR (difference between basal OCR and OCR after oligomycin blocks ATP synthase) (Figure 11J) without a concomitant increase in intracellular ATP concentration (Figure 11K), supporting the idea that a HS diet promotes inefficient oxidative phosphorylation in colonic crypts. In accord, HS diet increased the mitochondrial content and reactive oxygen species (ROS) of colonic crypt cells (epithelial cellular adhesion molecule, EPCAM<sup>+</sup>); however, the ratio of ROS to mitochondrial mass was not different, suggesting individual mitochondria are not respiring at an increased rate (Figure 11L–N). Rather HS-fed colonocytes are experiencing greater ROS and SRC likely owing to increased numbers or size of mitochondria. Together, our data suggest glycolytic and aerobic metabolism are uncoupled in colonic crypts and an inability to flexibly switch metabolism with shifts in nutrients may underlie the negative effects of HS diet on colonic epithelial regeneration.

To determine which cell types in colonic crypts were showing the greatest change in metabolism, we isolated Lgr5<sup>+</sup> ISCs from Lgr5 reporter mice (*Lgr5*<sup>eGFP-cre-ERT2</sup>) fed

HS or HF diet for 2 weeks and analyzed their metabolic capacity.<sup>1</sup> Similar to colonic crypts, we found a high reliance on oxidative respiration in ISCs, with very low levels of ECAR (Figure 12A–E). Basal OCR and ECAR did not differ in ISCs from HS- or HF-fed mice and there was a small, but not statistically significant, increase in SRC in ISCs from HS-fed mice (Figure 12B, D, and F), suggesting TA cells may contribute most to the increased SRC of crypts isolated from HS-fed mice. In addition, Lgr5<sup>+</sup> ISCs only showed a modest increase in mitochondrial mass and ROS (Figure 12G–I), further supporting that TA cells may contribute most to the altered metabolic phenotype caused by a HS diet.

To determine whether mice fed a HS diet showed these metabolic alterations owing to similar dysregulation of pyruvate metabolism, as seen in high-glucose-treated colonoids, we measured phosphorylated PDH expression by microscopy. We observed decreased phosphorylation of PDH in HS-treated colonic crypts compared with HF-treated mice (Figure 12J and K). However, with the introduction of DSS, the level of p-PDH in HF/DSS-treated crypts significantly decreased while HS/DSS-treated crypts maintained their levels of p-PDH (Figure 12J and K). Thus, increased p-PDH in HF-fed mice may enable greater metabolic flexibility because they can induce increased pyruvate oxidation when metabolic needs increase, such as during the early proliferative response to DSS. In contrast, HS-treated epithelium seems to be attempting to metabolize pyruvate at maximum efficiency, reducing their ability to adapt, should they require increased energy for proliferative regeneration.

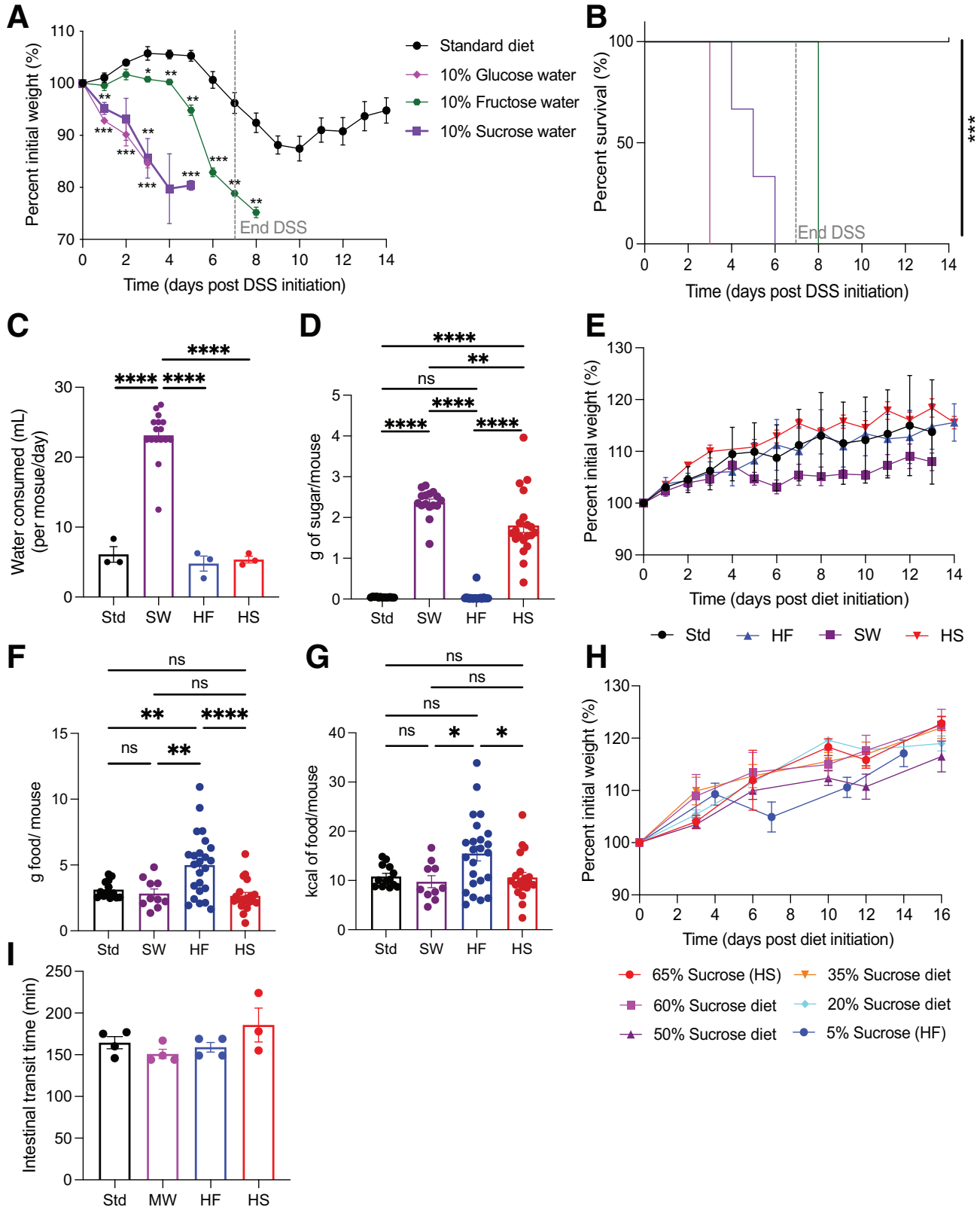
### HS Reduces Proliferative Potential of Lgr5<sup>+</sup> ISCs

Given the reduction in transcripts and gene sets associated with Lgr5<sup>+</sup> ISCs and TA cells in high-glucose-cultured colonoids, we postulated that a HS diet is specifically affecting these critical cells and their proliferative capacity in vivo. Using Lgr5 reporter mice,<sup>1</sup> we isolated Lgr5<sup>+</sup> ISCs and their immediate daughter TA cells (which retain low Lgr5 reporter expression) for RNAseq after 2 weeks of a HS or HF diet. At the transcriptome level, Lgr5<sup>+</sup> ISCs from mice fed different diets were only modestly different (Figure 13A–C). However, ISCs from HF-fed mice showed enrichment in the expression of proliferation-related genes

**Figure 6. (See previous page). The colonic epithelium can absorb luminal glucose, but do not express transporters to export glucose.** (A and B) *Lgr5*<sup>IRES-GFP-cre-ERT2</sup> mice were given a Cy5-glucose or anti-rat Cy5-secondary control enema for 30 minutes before being killed. (A) Representative images of colonic sections of individual and merged channels are shown. *White arrowheads* in magnified image show Cy5-glucose in Lgr5<sup>+</sup> ISCs. Images were taken at a magnification of 40× (scale bar: 20 μm). (B) Percentage Cy5<sup>+</sup> (glucose) colonic epithelial cells. Data are representative of 4 experiments and data points represent individual mice, error bars represent SEM. One-way analysis of variance was used to determine significance, where \*\**P* < .01 and \*\*\**P* < .001. (C–E) C57BL/6 or *Rag1*<sup>-/-</sup> mice were fed HS or HF diets for 2 weeks and then treated with DSS. (C) Bulk colonic epithelium was isolated from *Rag1*<sup>-/-</sup> female mice fed HS or HF diet for 2 weeks with or without 3 days of 3% DSS treatment, and transcriptome was assessed by RNAseq (n = 3–4). Glucose transporter expression level is shown. Data represent individual mice and error bars represent SEM. *Dotted line* represents no transcript. Blood glucose concentrations of HS- or HF-fed C57BL/6 mice: (D) postprandial and (E) fasted. Data are representative of 2–3 independent experiments (n = 3–4). Each data point represents individual mice, error bars represent SEM. (D) Mann–Whitney or (E) Student *t* test was used to determine significance. (F) FITC-dextran recovered from serum of HS- or HF-fed mice and from Std-fed mice treated with DSS for comparison. Data are representative of 2 independent experiments (n = 3), data points represent individual mice, error bars represent SEM. One-way analysis of variance was used to determine significance, where \**P* < .05. DAPI, 4',6-diamidino-2-phenylindole; FPKM, fragments per kilobase exon per million mapped reads.

targeted by Myc, a proto-oncogene, and E2F and in genes that make up the TA cell gene signature compared with ISCs from HS-fed mice (Figure 13A and D). Furthermore, the HS

diet enriched Lgr5<sup>+</sup> ISCs for genes associated with Notch inhibition, the major pathway inducing ISC stemness (Figure 13D). These data show that excess dietary sucrose is



sufficient to reduce the expression of transcriptional pathways involved in the proliferative potential of ISCs and the rapidly proliferating TA daughter cells.

### HS Impairs the Epithelial Proliferative Response to Damage

To better elucidate the consequences of HS-mediated impairment of metabolic and proliferative function of intestinal epithelium *in vivo*, we measured the transcriptome (RNAseq) of colonocytes from *Rag1*<sup>-/-</sup> mice (to ensure no intraepithelial lymphocyte contamination) fed HS or HF diets. Critically, lymphocytes are not required for the effects of HS because *Rag1*<sup>-/-</sup> mice phenocopy *C57BL/6* mice treated with DSS (Figure 14A and B). Diet alone induced few transcriptional changes when comparing colonocytes from HS- and HF-fed mice (Figure 14C–E). However, after 3 days of DSS damage, HS/DSS-treated mice had reduced expression of the core gene signatures of *Lgr5*<sup>+</sup> ISCs, TA cells, and secretory goblet cells, compared with HF/DSS-treated mice, similar to high-glucose-treated colonoids (Figures 1 and 14C and F). Genes associated with enteroendocrine cells were not affected, indicating a cell-type-specific effect (Figure 14C). GSEA confirmed these results because HF/DSS-treated epithelium was enriched for the ISC signature compared with HS/DSS-treated epithelium, as well as enriched for gene sets involved in cell-cycle progression and proliferation, including E2F targets, Growth 2 - Mitosis (G2-M) checkpoint, Myc targets, cell cycle, DNA repair, and mitotic spindle genes (Figure 14G). In contrast, epithelium from HS/DSS-treated mice showed an enrichment for the epithelial-mesenchymal transition gene set (Figure 14G), which is a characteristic pathologic progression in IBD patients, leading to fibrosis and strictures.<sup>39</sup> Typically, *Lgr5* expression and function is reduced by day 7 of DSS treatment, yet HS-fed mice lose *Lgr5* transcript expression by day 3 of DSS, indicating an accelerated disease progression (Figure 14C).<sup>40</sup> Confirming our transcriptional data, colonocytes from HS-fed mice expressed lower protein levels of the nuclear proliferative marker Ki67 after 3 days of DSS, showing reduced epithelial proliferation early after DSS damage (Figure 15A and B). There were no differences in terminal deoxynucleotidyl transferase-mediated deoxyuridine triphosphate nick-end labeling (TUNEL) and activated caspase-3 after 3 days of DSS treatment, indicating the HS

diet was not increasing colonocyte death (Figure 15C–E). Finally, by day 4 of DSS, HS/DSS-treated mice had fewer total colonocytes compared with HF/DSS-treated mice (Figure 15F), confirming impaired replacement of damaged epithelium. RNAseq analysis also showed significantly increased expression of glycolysis-regulating enzymes, such as *Hk2*, *Hk3*, and *Pfkfb3*, and of the most highly expressed isoforms of PDHK (*Pdk1* and *Pdk4*) in HS/DSS-treated epithelium compared with HF/DSS (Figure 14H), while nonregulatory enzymes of glycolysis and the TCA cycle were not affected consistently. Therefore, under high-sucrose conditions, DSS damage induces similar transcriptional changes in the epithelium as were observed in colonoids under high-glucose conditions (Figure 1).

Given the importance of replacing lost and damaged epithelium by ISCs and TA cells, we postulated that the HS diet impairs the early damage response to DSS damage. To show this, we traced the lineage of *Lgr5*<sup>+</sup> daughter cells using *Lgr5*<sup>eGFP-Cre-ERT2</sup>/*Rosa*<sup>LSL-TdTomato</sup> (TandemDimerTomato) mice after 3 days of DSS. HS/DSS-treated mice had reduced cell migration up crypt walls, as indicated by the distance and relative position of tamoxifen-activated Tomato<sup>+</sup> cells from green-fluorescent protein (GFP<sup>+</sup>) ISCs located at the base of the crypt, as well as fewer total Tomato<sup>+</sup> cells per GFP<sup>+</sup> crypt (Figure 15G–J). Furthermore, HS/DSS significantly reduces the number of 5-ethynyl-2'-deoxyuridine (EdU<sup>+</sup>) colonocytes and the greatest change in EdU accumulation was seen in the Tomato<sup>+</sup> compartment, or the immediate daughter cells that typically are proliferating rapidly (Figure 15K). Thus, similar to colonoid development, DSS-induced damage also requires active cycling of ISCs and migration of TA cells, which is impeded by dietary sucrose.

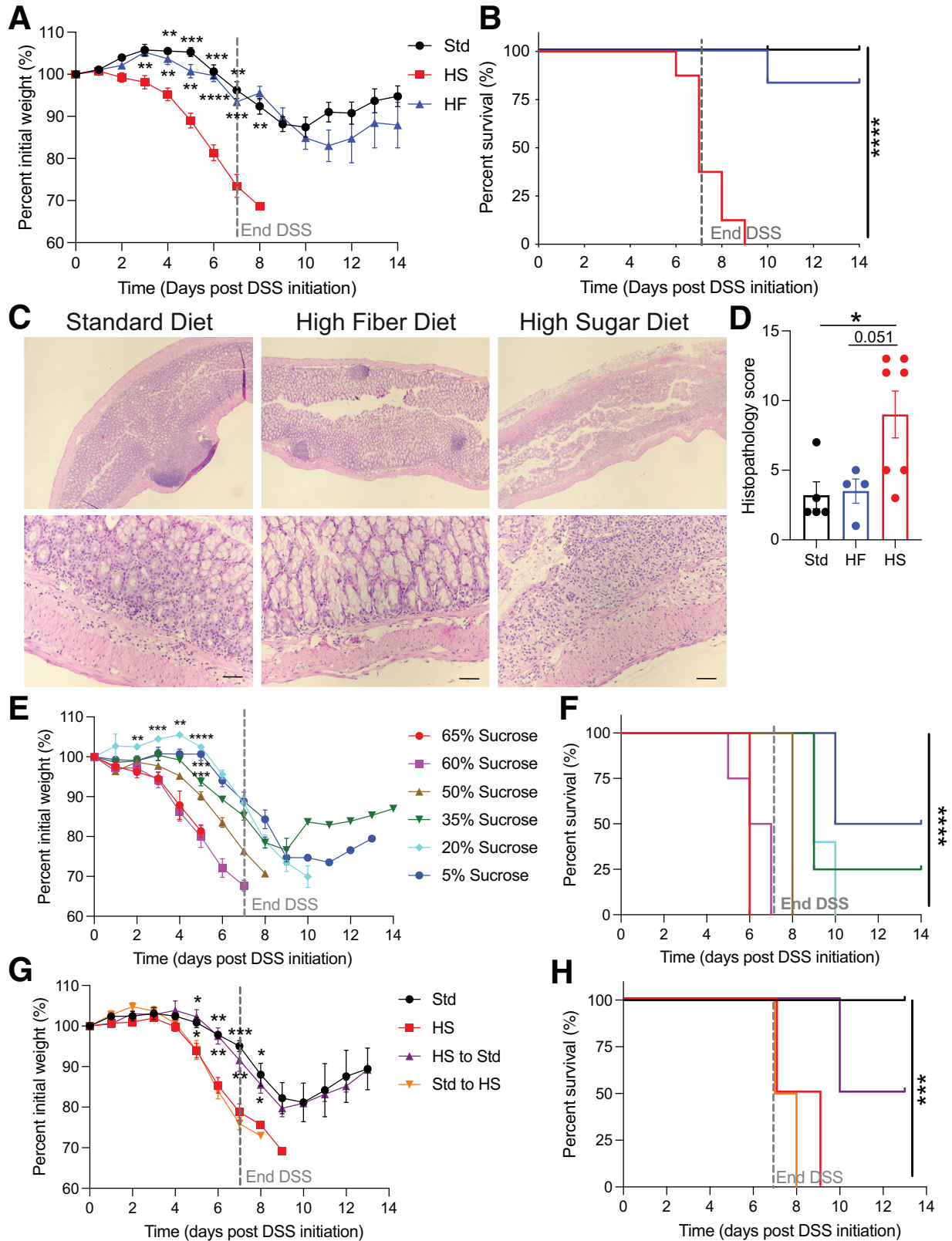
## Discussion

We report that sugar can directly impair the growth of ISCs into organized colonoids *in vitro* and leads to pyruvate accumulation and reduced ATP levels, suggesting that HS conditions substantially modify metabolism. By biochemically improving pyruvate to acetyl-CoA conversion and recoupling glycolysis to aerobic respiration, we restored ISC growth and colonoid development under high-sugar conditions. We confirmed the importance of these findings

**Figure 7. (See previous page). Sugar-supplemented water increases consumption and worsens DSS colitis. (A and B)** Five-week-old female *C57BL/6Tac* mice were fed standard diet and water containing 10% sucrose, glucose, or fructose for 2 weeks and then treated with 3% DSS drinking water (dotted line) for 1 week. (A) Percentage initial weight and (B) survival are shown. (C–H) Five-week-old female *C57BL/6Tac* mice were fed HS, HF, or standard (Std) diet with 10% sucrose-supplemented water (SW) for 2 weeks. (C) Volume of water, (D) grams of sugar consumed per mouse, (E) weight change, (F) grams of food consumed per mouse, (G) kcal from food consumed per mouse, and (H) weights of mice on respective diets were measured. Analysis of variance was used to determine statistically significant differences in food or sugar intake between groups using body weight as a covariable, where \**P* < .05. (I) Mice were fed HF, HS, or Std diet with 10% mannitol water (MW) for 2 weeks and gavaged with carmine dye. The time to intestinally pass the carmine dye was measured. Data points represent means ± SEM and are representative of 2 experiments (n = 3–4). Multiple *t* tests performed comparing to Standard-fed mice were used to determine significance, where \**P* < .05, \*\**P* < .01, \*\*\**P* < .001, and \*\*\*\**P* < .0001. (H) Five-week-old female *C57BL/6Tac* mice were fed diets with increasing concentrations of sucrose compared with fiber for 2 weeks. Weight change with different diets is shown. Kruskal–Wallis was used to determine significance.

in vivo, where colonic crypts from HS-fed mice had an increased glycolytic response to glucose deprivation that did not coincide with a requisite increase in respiration, and

Lgr5<sup>+</sup> ISCs from HS-fed mice had a reduced proliferative potential. Furthermore, we showed that these changes to the epithelium accelerate lethal colonic damage in HS/DSS-



treated mice and can induce worse disease independent of the microbiome. Finally, we showed that accelerated colonic disease is caused by a failed early proliferative response to injury resulting in fewer TA cells with reduced migration up crypt walls to restore the colonic barrier. Thus, high concentrations of sugar affect the ability of ISCs to proliferate to restore the colonic epithelium. In contrast high-sugar concentrations had little effect on mature colonoids or the steady-state colon, thus uncovering a distinct inhibitory role for dietary sucrose on the regenerative function of crypt ISCs and TA cells.

The exact metabolic mechanism behind the negative effect of HS on ISCs and TA cells is unclear. ISCs have distinct metabolic needs compared with most other cell types and, in the small intestine, require Paneth cells to produce lactate before transferring it to ISCs, where it is converted to pyruvate and used for respiration, supporting the hypothesis that glycolysis may have negative effects on ISC function.<sup>41,42</sup> Indeed, impaired fatty acid oxidation disrupts ISC self-renewal and ultimately results in loss of Lgr5<sup>+</sup> ISCs.<sup>12,43</sup> Excess cellular glucose also inhibits fatty acid oxidation by reducing carnitine palmitoyltransferase activity, which is the enzyme that esterifies fatty acids in preparation for transfer across the mitochondrial membrane for further oxidation.<sup>44,45</sup> By blocking PDHK with DCA, pyruvate conversion to acetyl-CoA and flux through the TCA cycle were increased and colonoid development was restored. However, DCA is poorly bioavailable and affects multiple critical organ systems in vivo,<sup>46</sup> resulting in inconsistent results when we tried to use it to reverse disease in HS-treated mice (data not shown). As cells undergo differentiation, they characteristically increase mitochondrial copy number, SRC, and ROS, while stem cells and proliferating cells maintain a lower SRC.<sup>42</sup> Thus, our data showing increases in mitochondria, SRC, and ROS in ISCs and TA cells in high-sucrose conditions indicate that they may be experiencing premature differentiation. Metabolites also can control stem cell fate epigenetically via acetyl-CoA levels, which promote histone acetylation during stem cell self-renewal and might be important for epithelial regeneration after damage.<sup>47</sup>

Epidemiologic studies have found a positive association of IBD and high consumption of dietary sugar and sweetened beverages.<sup>48,49</sup> Mice that consume a diet high in sugar have worse disease in models of colitis,<sup>50–52</sup> and clinical trials that significantly reduce dietary sugar have already shown promise in reducing disease burden in IBD patients in the pediatric intensive care unit.<sup>53–55</sup> Treatment of active

flares of pediatric Crohn's disease often involve exclusive enteral nutrition; in contrast, exclusive enteral nutrition is not an indicated treatment for acute ulcerative colitis flares.<sup>56</sup> Given that DSS damage is most representative of the colonic damage seen in acute flares of ulcerative colitis, perhaps we have uncovered a mechanism by which exclusive enteral nutrition, which can contain high amounts of sugar and emulsifiers, is ineffective in ulcerative colitis patients.<sup>57</sup> Given the direct effects of dietary components on the health and function of intestinal epithelium, it is imperative that we better understand how different dietary components may impact the regenerative capacity of the intestinal epithelium to better treat patients showing high levels of intestinal damage, whether it be from infection, auto-inflammation, or radiation.

## Materials and Methods

### Resource Sharing

Data (including sequencing) and analytic methods will be made available upon request.

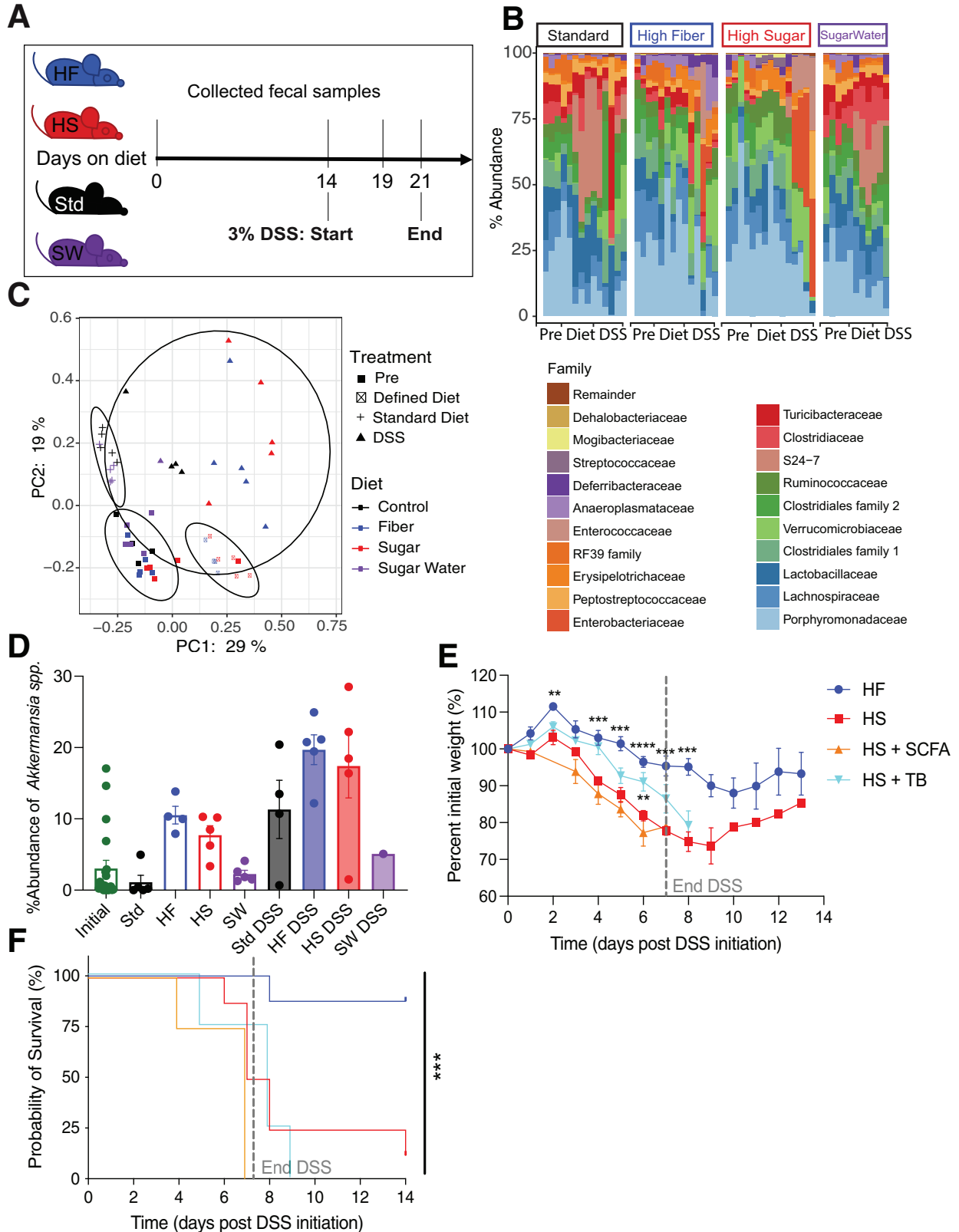
### Mouse Crypt-Derived Organoid Generation

Mouse intestinal crypt-derived organoids were generated as described previously.<sup>5</sup> Briefly, 8- to 12-week-old mice were killed with CO<sub>2</sub>. The whole intestine was extracted and cleaned from fat, connective tissue, blood vessels, and flushed with ice-cold phosphate-buffered saline (PBS). The intestine was cut into smaller pieces after lateralization and incubated in 7.5 mmol/L EDTA in ice-cold PBS with mild agitation for 45 minutes at 4°C. Then, the crypts were mechanically dissociated from tissue via shaking and strained through a 40- $\mu$ m strainer. After washing with ice-cold PBS and centrifugation at 300 r.c.f. (relative centrifugal field) for 5 minutes in a microcentrifuge (0540390; Thermo Fisher), isolated crypts were counted and embedded in Matrigel (356231, Growth Factor Reduced; Corning) in a 1:4 ratio at 5–10 crypts per microliter and plated in 24-well plates (25  $\mu$ L dome/well). The Matrigel was allowed to solidify for 8–15 minutes in a 37°C incubator and solidified domes were cultured in Advanced Dulbecco's modified Eagle medium (DMEM; Gibco) media supplemented with recombinant murine chiron 10  $\mu$ mol/L (Stemgent), noggin 200 ng/mL (Peprotech), R-spondin 500 ng/mL (R&D or Sino Biological), N2 1 $\times$  (Life Technologies), B27 1 $\times$  (Life Technologies), Y-27632 dihydrochloride

**Figure 8.** (See previous page). Excess dietary sucrose leads to lethal DSS-induced colonic damage. (A–D) C57BL/6 mice were fed Std, HF, or HS diets for 2 weeks and then treated with 3% DSS drinking water for 1 week. (A) Percentage initial weight and (B) survival shown. (C) Representative H&E of colonic sections taken on day 6 of DSS (magnification, 4 $\times$  and 20 $\times$ ; scale bar: 50  $\mu$ m). (D) Histopathology score of blinded H&E sections, where scores of 1–5 indicate mild colitis, 6–10 indicate moderate colitis, and 11–17 indicate severe colitis. Kruskal–Wallis was used to determine significance, where \* $P$  < .05. (E and F) Mice fed diets with increasing concentrations of sucrose compared with fiber for 2 weeks and treated with DSS for 1 week. (E) Percentage initial weight and (F) survival shown. (G and H) Mice were fed 2 weeks of Std diet and switched to HS on the first day of DSS treatment (purple) or fed 2 weeks of HS then switched to Std diet on the first day of DSS (orange). (G) Percentage initial weight and (H) survival are shown. Data are representative of 3 experiments ( $n = 2–4$ ) and data points represent means  $\pm$  SEM. Multiple  $t$  tests were performed against HS per day using multiple comparisons and FDR < 0.01, where \* $P$  < .05, \*\* $P$  < .01, \*\*\* $P$  < .001, and \*\*\*\* $P$  < .0001.

monohydrate 20 ng/mL (Sigma-Aldrich), epidermal growth factor (EGF) 40 ng/mL (R&D), and N-acetyl-L-cysteine 1 μmol/L (Sigma-Aldrich). A total of 500 μL

crypt media was changed every other day and maintained at 37°C in a fully humidified chamber containing 5% CO<sub>2</sub>.





### Mouse Organoid Propagation

Organoids were propagated by dissociating crypt-derived organoids in TrypLE Express (Invitrogen) for 3 minutes at 37°C. After this time, the TrypLE Express was quenched by adding 1–2 times that amount of Advanced DMEM/F12 (Gibco). The pellet containing the dissociated intestinal single cells after centrifugation in a microcentrifuge (0540390; Thermo Fisher) at 300 r.c.f. for 5 minutes was resuspended in Matrigel (356231 Growth Factor Reduced; Corning) and embedded onto a flat-bottom, 24-well cell culture plate (3526; Corning) by forming 20- $\mu$ L droplets of Matrigel, creating at least 3 technical replicates for each condition. The embedded Matrigel droplets were immediately placed inside a fully humidified incubator containing 5% CO<sub>2</sub>, which was maintained at 37°C for 5 minutes to solidify the Matrigel droplets. Once the Matrigel was solidified, 600  $\mu$ L supplemented Advanced DMEM/F12 cell medium described earlier was added to each well. The media was changed every 2 days for each well and the plate was maintained in a 37°C incubator.

### Human Patient-Derived Colon Organoid Generation

Human colon organoids were generated as described previously with minor modifications.<sup>5</sup> Briefly, normal colon tissue samples were obtained from patients with informed consent undergoing surgical resection procedures at Northwell Health. Study protocols were reviewed and approved by the Northwell Health Biospecimen Repository (1810). Tissue samples were first cut into small pieces, approximately 0.5 cm<sup>2</sup>, and incubated at 4°C in an antibiotic mixture consisting of 1 $\times$  PBS + 100  $\mu$ g/mL normocin (cat# ant-nr-1; Invivogen), 50  $\mu$ g/mL Gentamicin (cat# E737; Amresco), and 1 $\times$  Penicillin-Streptomycin, (cat# 15070063; ThermoFisher) for 15 minutes. Next, the pieces were washed with 1 $\times$  PBS before a 75-minute incubation in a 5-mmol/L EDTA solution at 4°C on a rocker. After incubating, the tissue samples were washed once more with 1 $\times$  PBS. Crypts then were released from the tissue by shaking the pieces in a tube with ice-cold 1 $\times$  PBS. Crypts in the supernatant were transferred to a new tube and spun down at 100  $\times$  *g* for 5 minutes at 4°C. These isolated crypts then were embedded in a 70/30 Matrigel (cat# 356231; Corning) and culture medium mixture and plated in 40- $\mu$ L droplets on 12-well plates. The Matrigel was allowed to polymerize at 37°C for

15 minutes before adding 1 mL culture medium to each well, with the culture medium consisting of Advanced DMEM (12634028; Life Technologies), 1 $\times$  GlutaMAX (35050061; Life Technologies), 10 mmol/L HEPES (15630080; Thermo Fisher Scientific), 50% WRN-conditioned medium,<sup>50</sup> 1 $\times$  B27 (12587010; Life Technologies), 1 $\times$  N2 (17502048; Life Technologies), 10 mmol/L nicotinamide (N0636; Sigma Aldrich), 1 mmol/L N-acetyl cysteine (A9165; Sigma Aldrich), 100  $\mu$ g/mL<sup>-1</sup> Primocin (ant-pm-1; Invivogen), 10  $\mu$ mol/L SB202190 (S7067; Sigma Aldrich), 10  $\mu$ mol/L Y-27632 (1254; Tocris), 10 nmol/L gastrin I (G9020; Sigma Aldrich), 50 ng mL<sup>-1</sup> EGF (AF-100-15; Peprotech), and 500 nmol/L A83-01 (SML0788; Sigma Aldrich).

### Human Patient-Derived Colon Organoid Propagation

Human colon organoids were dissociated in Cell Recovery Solution (354253 Growth Factor Reduced; Corning) for up to 1 hour at 4°C. Once the Matrigel was dissolved, the organoids were spun at 500 r.c.f. for 5 minutes at 4°C. The supernatant was removed and the pellet was resuspended in TrypLE Express (12604039; ThermoFisher). After a 5-minute incubation at 37°C, the digestion was stopped by adding Advanced DMEM. The solution then was centrifuged at 500 r.c.f. for 5 minutes at 4°C. Dissociated cells were seeded in 40- $\mu$ L Matrigel droplets and culture medium mixture. Culture medium then was added to each well after the domes polymerized.

### Sugar Dose Response in Organoids

Dose-response experiments using organoids were performed using additional D(-)-fructose (F0127; Sigma-Aldrich), D-(+)-glucose (G7528; Sigma-Aldrich), sucrose (S0389; Sigma-Aldrich) at 200, 100, 50, 25, 12.5, 3.1, and 0.8 mmol/L concentrations (equaling 225, 125, 75, 50, 37.5, 28.1, and 25.8 mmol/L of glucose, respectively, adding in the base amount in DMEM). Briefly, normal colon organoids were dissociated to near-single cells and plated onto a 24-well plate, with 20- $\mu$ L domes per well. A total of 500  $\mu$ L culture medium further supplemented with different concentrations of D(-)-fructose (F0127; Sigma-Aldrich), D-(+)-glucose (G7528; Sigma-Aldrich), or sucrose (S0389; Sigma-Aldrich) was added to each well at the time of seeding. Media with the supplemented sugars was refreshed every 2 days, and growth was followed up to day 12. Alternatively, normal colon organoids were

**Figure 9.** (See previous page). **Effects of dietary sugar on the colonic microbiota.** (A–D) C57BL/6 mice were fed HS or HF diets for 2 weeks and then treated with DSS, fecal samples were collected for 16S rRNA amplicon sequencing. (A) Schematic of diet/DSS treatment and days fecal samples were collected for 16S rRNA analysis. (Pre, day mice arrived at facility; Diet, 14 days of respective diet [sucrose-supplemented water (SW), Std with 10% sucrose in water]; DSS, collected during DSS treatment). (B) Relative abundances of the top 20 most abundant families. (C) Ordination plot based on the principle coordinate analysis (Bray–Curtis) shows taxonomic variations of microbial communities with various diet treatments (defined diets: HF and HS; standard diet: Std and SW). (D) Relative abundance of *Akkermansia* species as determined by 16S rRNA gene sequencing. (E and F) Mice fed HF, HS, or HS with SCFA supplementation in the water or tributyrin (TB)-supplemented HS diet for 2 weeks and then treated with DSS for 1 week. (E) Weight loss and (F) survival are shown. Data are representative of 2–3 independent experiments (*n* = 4). Data points represent means  $\pm$  SEM. Multiple *t* tests were performed against HS per day, where \*\**P* < .01, \*\*\**P* < .001, \*\*\*\**P* < .0001. PC, Principal Coordinate.

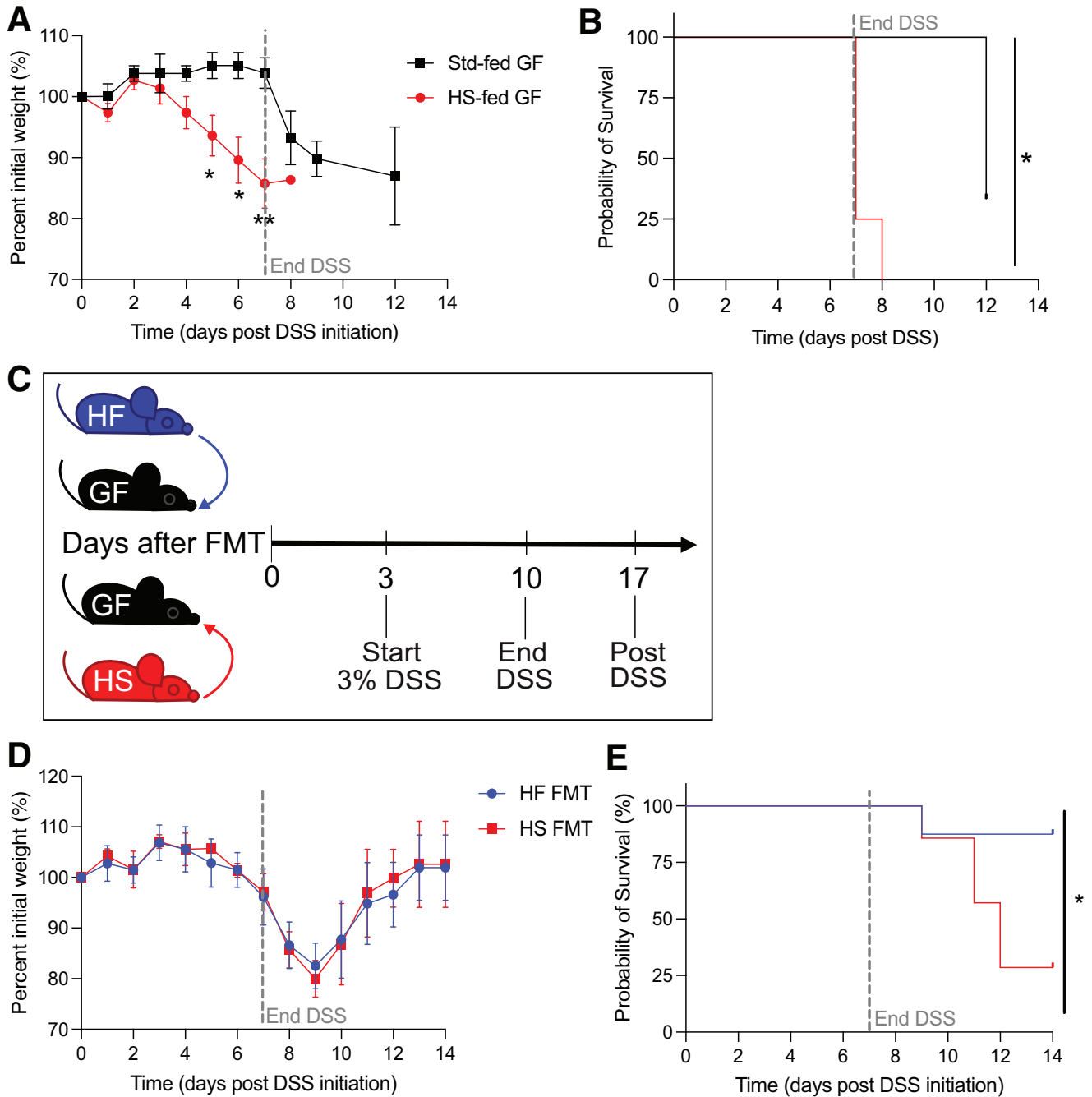


**Figure 10. HS diet induces lethal colitis independent of changes to the microbiota.** (A and B) Germ-free mice were fed HS or Std diet for 2 weeks, then treated with 1% DSS for 1 week. (A) Percentage initial weight and (B) survival curve are shown. (C–E) Germ-free female C57BL/6 mice were gavaged with FMT from mice fed HS or HF diet for 2 weeks. After 3 days of intestinal colonization, mice were treated with 3% DSS drinking water for 1 week. (C) Schematic of FMT and DSS treatment. (D) Weight loss and (E) survival were measured. Data points represent means  $\pm$  SEM from 2 independent experiments ( $n = 4$ ) and  $*P < .05$ ,  $**P < .01$ . GF, germ-free.

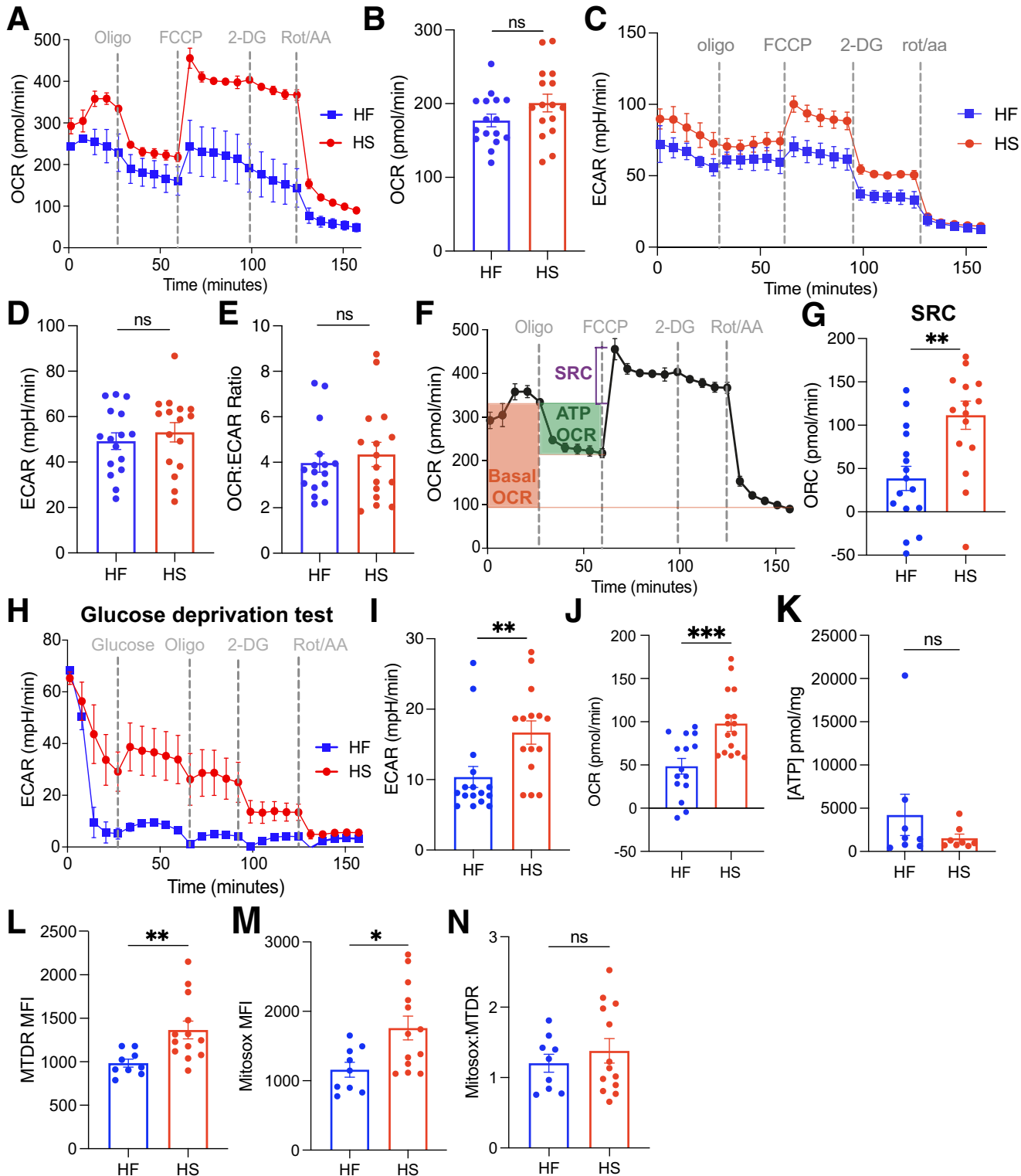
dissociated to near-single cells and plated onto a 24-well plate, with 20- $\mu$ L domes per well. A total of 500  $\mu$ L standard culture medium was added and organoids were allowed to grow to day 5. Media then was changed to media supplemented with additional glucose, fructose, or sucrose at varying concentrations. Growth was followed up for the next 48 hours.

### Murine Intestinal Organoid Intracellular Metabolite Isolation

Unless otherwise stated, the dissociation, centrifugation, embedding of Matrigel droplets, media addition, and incubator use are the same as indicated for the murine intestinal organoid culture. For metabolite analysis, organoids were dissociated as described and cells were seeded in a 1.5-mL

10% Matrigel/90% mouse organoid culture medium slurry for each condition in separate 24-well plates. The medium for the low-glucose condition was supplemented with an additional 25 mmol/L glucose (G7021; Sigma, totaling 50

mmol/L) and the medium for the high-glucose condition was supplemented with an additional 100 mmol/L glucose (totaling 125 mmol/L) with and without 4 mmol/L sodium DCA (347795; Sigma). These plates were spun at  $100 \times g$



for 1 minute at 4°C in a centrifuge (022623508; Eppendorf) to allow settling of cells to the bottom of the wells. Then, both plates were placed in a fully humidified 37°C incubator. For negative control, empty wells were filled with 1.5 mL 10% Matrigel/90% murine organoid medium supplemented with 25 mmol/L or 100 mmol/L glucose with and without 4 mmol/L DCA.

On day 4 of culture, organoid medium from each well per condition and the blank wells were placed into Eppendorf tubes and snap-frozen in liquid nitrogen. A total of 800  $\mu$ L 1  $\times$  PBS was used to mix and collect the organoids from each experimental well into Eppendorf tubes and these were spun at 300  $\times$  *g* for 1 minute at 4°C. After centrifugation, each tube containing the organoid pellet had its supernatant aspirated without disturbing the pellet. Metabolite extraction solution (1 mL, stored at -80°C) consisting of 50% methanol stock (322415; Sigma), 30% acetonitrile stock (A998N1; Fisher), and 20% distilled water was added to each pellet and mixed thoroughly. Once mixed, each tube containing the extraction solution was snap-frozen in liquid nitrogen, thawed, and then snap-frozen in liquid nitrogen again.

The thawed tubes were mixed at maximum speed on a thermomixer (538200023; Eppendorf) set to 4°C for 15 minutes. After mixing, they were incubated overnight at -80°C. The next day, these tubes were centrifuged for 10 minutes at maximum speed at 4°C and the supernatant was collected into Eppendorf tubes while the pellets were kept on ice. This collected supernatant then was centrifuged for 10 minutes at maximum speed at 4°C and its supernatant was decanted into autosampler vials (29659-U; Sigma), which then were incubated at -80°C until metabolite analysis. A total of 300  $\mu$ L of 0.1 mol/L NaOH was added to each tube containing an organoid pellet and was mixed thoroughly followed by maximum speed incubation for 15 minutes at 4°C on a Thermomixer (Eppendorf). These tubes then were centrifuged at 300  $\times$  *g* for 5 minutes at 4°C and the supernatants were used for protein quantification using the Detergent Compatible protein quantification assay protocol (5000112; Bio-Rad). After incubation at -80°C for 1 hour, samples were centrifuged to remove the precipitated proteins and insoluble debris. The

supernatants were collected and stored in autosampler vials at -80°C until analysis.

Samples were randomized to avoid bias resulting from machine drift and processed blindly. Liquid chromatography–mass spectrometry analysis was performed using a Vanquish Horizon UHPLC (Ultra-High-Performance Liquid Chromatography) system coupled to a Q Exactive HF (high field) mass spectrometer (both Thermo Fisher Scientific). Sample extracts were analyzed as previously described.<sup>51</sup> The acquired spectra were analyzed using XCalibur Qual Browser and XCalibur Quan Browser software (Thermo Fisher Scientific) by referencing an internal library of compounds.

### Western Blot of Murine Intestinal Organoids in High-Glucose Treatment

After 6 days of culture in 100 mmol/L or 25 mmol/L of added glucose (totaling 125 mmol/L and 50 mmol/L, respectively), culture media was removed, colonoids were incubated in cold 0.5% bovine serum albumin (BSA) in PBS for 1 minute to dissolve Matrigel, and spun at 150  $\times$  *g* for 5 minutes at 4°C. Colonoid pellet was washed in 0.5% BSA in PBS and spun twice more and then resuspended in 70  $\mu$ L RIPA buffer with phosphatase/antiprotease inhibitors and left on ice for 30 minutes. Samples were spun and supernatant was stored in -80°C overnight, and then boiled with Laemmli buffer for 5 minutes at 95°C. The amount of protein to load was determined based on heat shock protein 90 band intensities from an initial trial blot. Samples then were probed for phospho-PDH (Ser 293, ref 31866; Cell Signaling), PDH (ref 2784; Cell Signaling), and heat shock protein 90 (C45G5, ref 4877; Cell Signaling) overnight in 5% nonfat dried milk at 4°C.

### Sugar and Inhibitor Treatment in Murine Intestinal Organoids

Unless otherwise stated, the dissociation, centrifugation, embedding of Matrigel droplets, media addition, and so forth were the same as indicated previously for colonoids. Glucose, sucrose, fructose, and inhibitor drugs were added into the cell medium (250  $\mu$ L for each well) of a flat-bottom, 48-well culture plate (3526; Corning) containing previously

**Figure 11.** (See previous page). High-sucrose diet increases spare respiratory capacity of colonic crypt cells. (A–J) Colonic crypts isolated from mice fed HS or HF diet for 2 weeks and plated on a Matrigel-coated Seahorse XF analyzer plate. (A) Representative OCR trace and (B) quantification of basal OCR (average OCR before oligomycin addition). (C) Representative ECAR trace after and (D) quantification of basal ECAR (average ECAR before oligomycin addition). (E) OCR to ECAR ratio, using basal rates from panels B and D. (F) Schema of how SRC, ATP-associated OCR, and basal OCR were measured. (G) Quantification of SRC (difference between basal and maximal oxidative rates, achieved after FCCP injection). (H) Representative ECAR trace after 3-hour glucose deprivation and (I) glycolytic rate measured by subtracting basal rate after 2-deoxyglucose (2-DG) injection from maximum response after glucose injection. (J) Tabulated ATP-associated OCR (difference between basal OCR and OCR after oligomycin injection). (K) Five-week-old C57Bl/6 female mice were fed HS or HF diet for 2 weeks, the colonic epithelium was isolated, and ATP concentration was measured. (L–N) *Lgr5*<sup>eGFP-Cre-ERT2</sup> reporter mice were fed HS or HF diet for 2 weeks and colonic crypts were dispersed to single cells or fixed for microscopy and fluorescently stained. (L) Mean fluorescent intensity of MitoTracker Deep Red (MTDR MFI) and (M) MitoSox for all EPCAM<sup>+</sup> cells. (N) Ratio of MitoTracker Deep Red MFI to MitoSox MFI in EPCAM<sup>+</sup> cells. Data are representative of 2–4 experiments (*n* = 2–4) and data points represent means  $\pm$  SEM. Tabulated bar charts represent means  $\pm$  SEM, with each point representing 1 mouse. (E, J, and K) Significance was determined by Student *t* test or Mann–Whitney, where \**P* < .05, \*\**P* < .01, \*\*\**P* < .001. Metabolic inhibitors used were oligomycin (oligo), FCCP, 2-DG, and rotenone with antimycin (rot/aa).

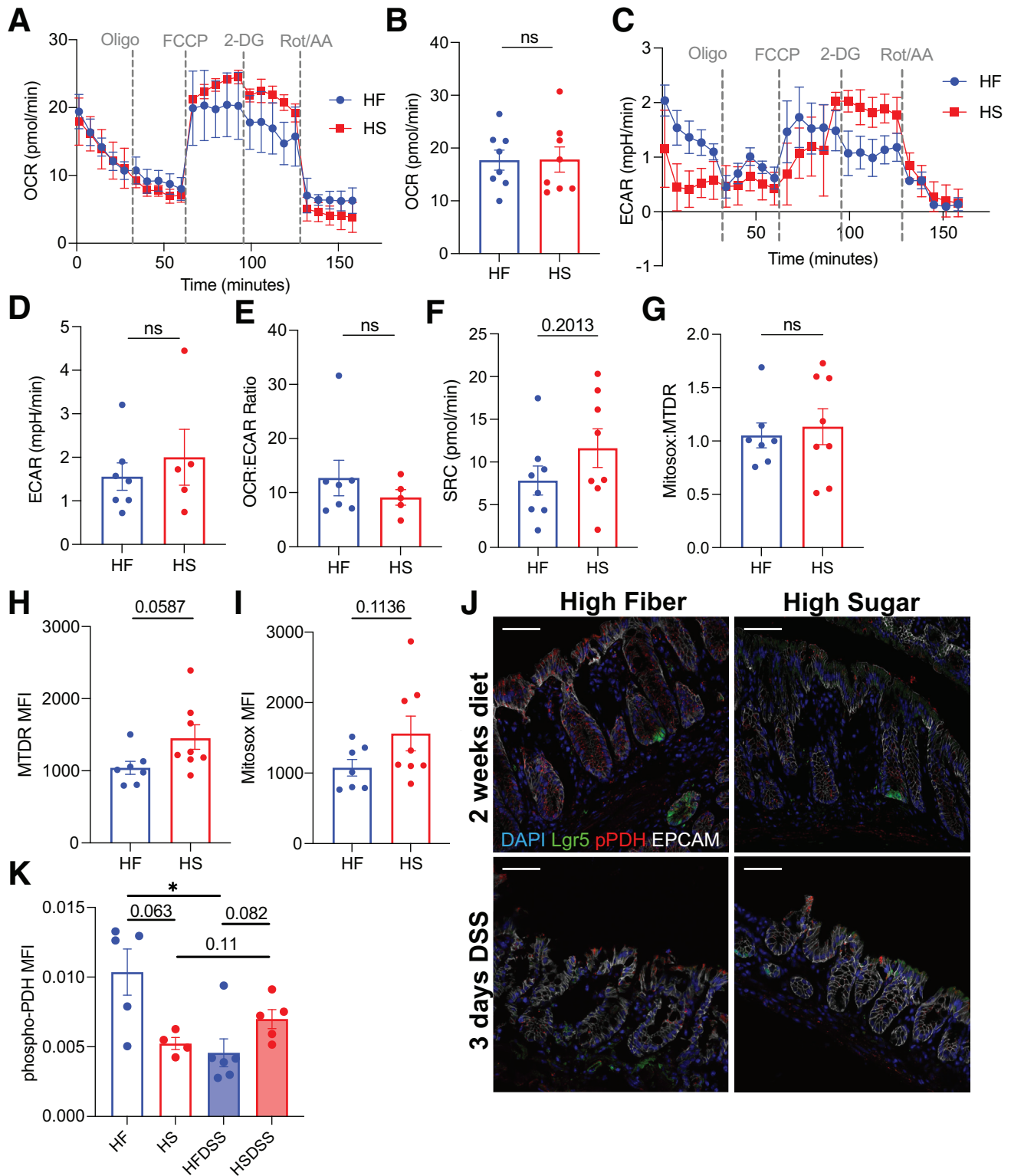


**Figure 12. Metabolic changes in colonic ISCs with increased dietary sucrose.** (A–I) *Lgr5*<sup>HRES-GFP-cre-ERT2</sup> mice were fed HS or HF diet for 2 weeks, and colonic epithelium was isolated and stained for flow cytometry. (A–F) *Lgr5*<sup>+</sup> ICSs were sorted for metabolic analysis on a Seahorse XF analyzer. (A) Representative trace of OCR, (B) tabulated basal OCR, (C) representative trace of ECAR, (D) tabulated basal ECAR, and (E) ratio of basal OCR to ECAR (taken from panels B and D). (F) Tabulated SRC (difference between basal and maximal oxidative rates, achieved after FCCP injection). (G) Ratio of MitoTracker Deep Red mean fluorescence intensity (MFI) to MitoSox MFI in *Lgr5*<sup>+</sup> cells. (H) MFI of MitoTracker Deep Red (MTDR) and (I) MitoSox for *Lgr5*<sup>+</sup> cells. Data points represent individual mice, means ± SEM from 4 independent experiments (n = 2–4) are shown. (E) Student *t* test or Mann–Whitney test used to determine significance. Metabolic inhibitors used were oligomycin (oligo), FCCP, 2-deoxyglucose (2-DG), and rotenone with antimycin (Rot/AA). (J) Representative images of p-PDH staining (±HS diet, ±DSS; 3 days) and (K) quantification of the level of p-PDH MFI in crypt base cells (magnification, 40×; scale bars: 50 μm). Data are representative of 2 independent experiments (n = 2–3). Data points represent means ± SEM. Kruskal–Wallis was used to determine statistical significance, where \**P* < .05. DAPI, 4',6-diamidino-2-phenylindole.

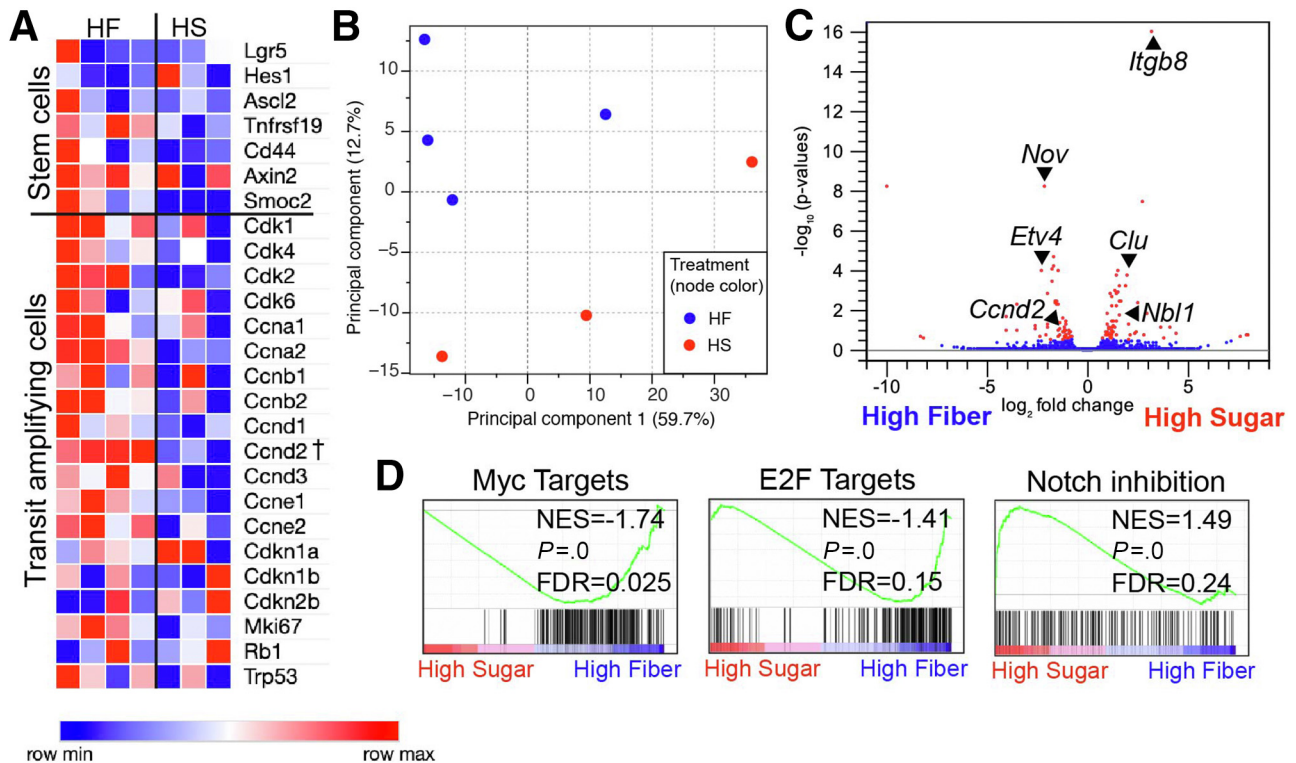


**Figure 13. HS diet reduces expression of proliferation-related genes in  $Lgr5^+$  ISCs.** (A–D)  $Lgr5^+$  ISCs were isolated by flow cytometry from  $Lgr5^{eGFP-Cre-ERT2}$  HS- or HF-fed mice and analyzed by RNAseq. (A) Transcript expression level of epithelial subset gene signatures and (B) Principal Component Analysis (PCA) plot showing variance with percentages on axes representing the percentage variance explained by each principle component. (C) Volcano plot for genes comparing HS- or HF-treated samples, where red points represent differentially expressed genes ( $-1.5 > FC > 1.5$ ;  $*P < .05$ ;  $FDR < 0.3$ ). (D) GSEA of  $Lgr5^+$  ISC RNAseq data showing enrichment of genes in HF-fed or HS-fed mice for gene sets indicated. For heatmap, dagger represents DEG in HS vs HF  $Lgr5^+$  ISCs ( $-1.5 > FC > 1.5$ ;  $*P < .05$ ;  $FDR < 0.3$ ). FDR, False Discovery Rate; max, maximum; min, minimum; NES, Normalized Enrichment Score.

passed colonoids and then dispersed into single cells. To test the effect of each chemical inhibitor we performed an initial dose-response curve. The concentrations determined from the dose response were as follows: 150 mmol/L glucose (totaling 175 mmol/L for all), 150 mmol/L fructose, 150 mmol/L sucrose, 7.8 nmol/L rotenone (R8875; Sigma), 1 mmol/L 2-deoxy-D-glucose (D8375; Sigma), and 4 mmol/L sodium dichloroacetate (347795; Sigma). After embedding the Matrigel domes and solidification, cell medium containing these doses of chemicals was added with 3 technical replicates per condition, including a control containing only the supplemented Advanced DMEM/F12 stated previously. From time zero to time 6 hours, the wells that were supposed to have sugars and inhibitors added together had only the inhibitors added to inhibit the cells and the wells that were supposed to have only sugars added had the control supplemented media added. After 6 hours, the sugars were added alone and with inhibitors to those respective wells. The media for this plate also was changed every 2 days. After 6 days in culture, organoid numbers and sizes were quantified and CellTiter-Glo values were obtained and plotted as a percentage of the control luminescence (Promega, Luminescent Cell Viability Assay, G7570).

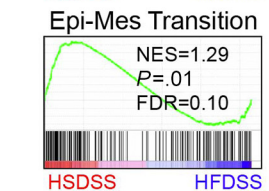
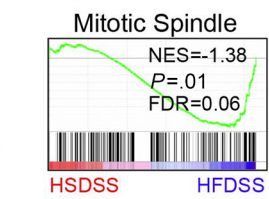
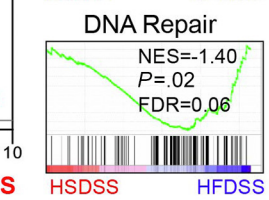
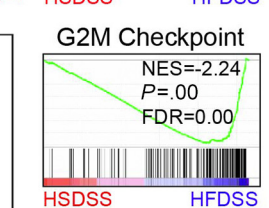
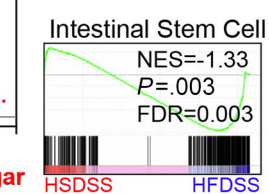
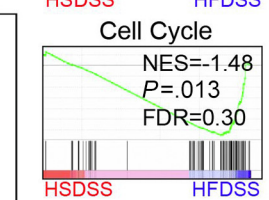
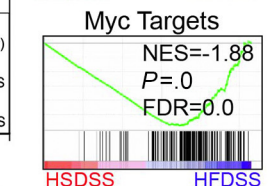
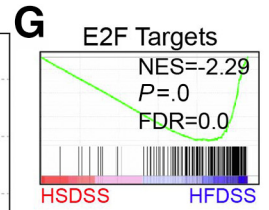
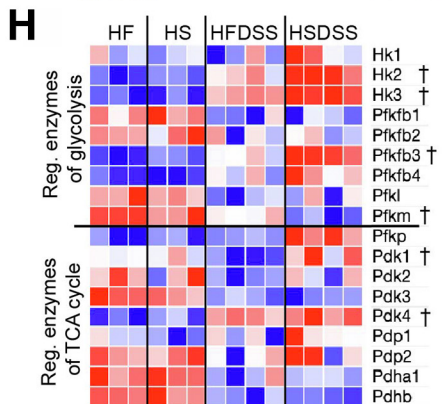
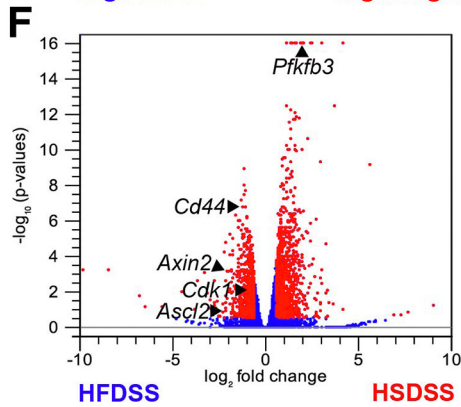
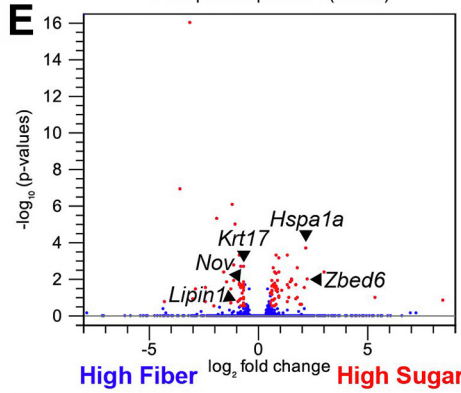
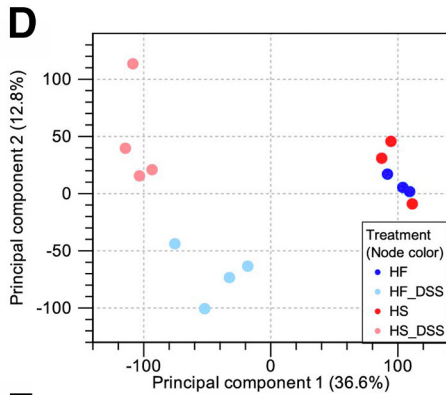
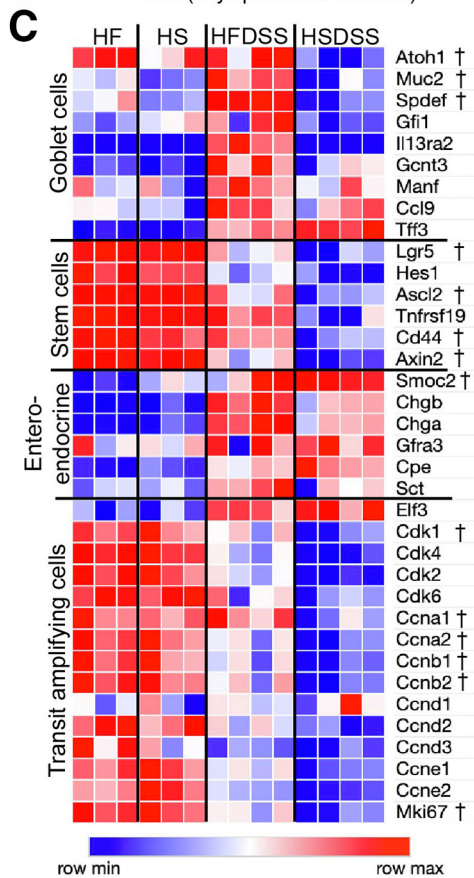
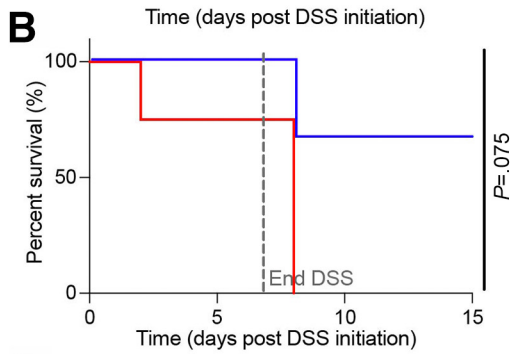
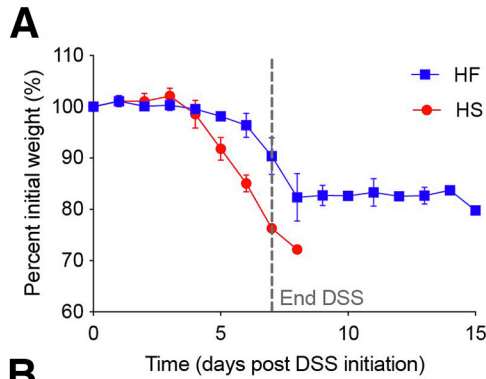
### Gene Expression Profiling by RNAseq and Bioinformatics Analyses

Cultured colonoids were grown in the conditions listed earlier and their RNA was extracted via TRIzol separation (Invitrogen, 15596018).

Colonic  $Lgr5^+$  cells were isolated from  $Lgr5^{eGFP-IRES-Cre-ERT2}$  (endogenous-green-fluorescent-protein-internal-ribosome-entry-site-Cre-recombinase-Estrogen-receptor-T2) reporter mice fed defined diets for 2 weeks, as described previously with some modifications.<sup>6</sup> Briefly, colons were butterflyed and vortexed to remove luminal contents, and then incubated at 37°C for 30 minutes in EDTA to dissociate the epithelium from the lamina propria. Crypts were vortexed and passed through a 20-gauge needle to dissociate further into single-cell suspension were passed over a 20- $\mu\text{m}$  filter to further break up remaining clumps of cells. Cells were stained with a live/dead discrimination dye and antibodies against EPCAM (clone G8.8, catalog #563478; BD Biosciences) and CD45.2 (clone 104, ref 47-0454-82; Invitrogen) and then resuspended in rock-inhibitor containing DMEM to prevent differentiation of ISCs. Live cells were sorted on the MoFlo Astrios (Beckman) cell sorter directly into Takara kit lysis buffer (SmartSeq HT).

Bulk epithelium was isolated by scraping the apical side of the colonic tissue to release cells and placing in TRIzol to isolate RNA from *Rag1*<sup>-/-</sup> mice fed defined diets for 2 weeks

and either untreated (n = 3) or treated with 3 days of 3% DSS drinking water (n = 4). Samples isolated from DSS-treated mice were precipitated overnight in lithium



chloride to remove DSS, which may interfere with the sequencing process. DNA libraries were prepared (Nextera XT kit) and RNAseq was performed on an Illumina Next-Seq500 by the University of Pittsburgh Health Sciences Sequencing Core. Adapter sequences were trimmed from raw reads using Trimmomatic with default parameters. TopHat2.1.1 was used to map trimmed reads onto mouse genome build mm10 and Cufflinks was used to calculate gene expression values (fragments per kilobase exon per million mapped reads).<sup>52,58</sup> Enrichment of gene sets was calculated using GSEA from the Broad Institute (<http://www.broad.mit.edu/gsea>). Heatmaps were created using Morpheus from the Broad Institute (<https://software.broadinstitute.org/morpheus>) from fragments per kilobase exon per million mapped reads log<sub>2</sub> transformed expression levels.

### Mouse Models and Treatments

Five-week-old wild-type *C57BL/6Tac* mice (B6 MPF; Taconic) were used for diet and DSS treatment unless otherwise noted. *Lgr5<sup>eGFP-Cre-ERT2</sup>* mice (008875; Jackson Laboratories) were bred with *Rosa<sup>TdTomato</sup>* (007909; Jackson Laboratories) mice. *Rag1<sup>-/-</sup>* mice (002216) were purchased from Jackson Laboratories and bred in our facility. Both male and female age-matched mice (5–8 wk) were used for all experiments. All experiments were performed in an American Association for the Accreditation of Laboratory Animal Care-accredited animal facility at the University of Pittsburgh. Mice were kept in specific pathogen-free conditions and housed in accordance with the procedures outlined in the Guide for the Care and Use of Laboratory Animals under an animal study proposal approved by the Institutional Animal Care and Use Committee of the University of Pittsburgh. Upon arrival from Taconic, mice were placed on 2 special diets (HS, TD.160477 and HF, TD.160476; Envigo, Madison, WI) (Table 1). Mice were provided food ad libitum for 2 weeks and then provided DSS at 3% by weight in their drinking water ad libitum for 1 week. Mice were weighed daily during the initial diet change phase and daily once DSS was initiated, and for 1 week after changing DSS water back to untreated water. Gnotobiotic C57BL/6 female 8-week-old mice were housed in germ-free conditions and fed a sterilized HS or Std diet for 2 weeks, then treated with sterile 1% DSS drinking water ad

libitum, and weights were recorded daily throughout the experiment. Gnotobiotic C57BL/6 female 8-week-old mice were housed in germ-free conditions and then gavaged with the microbiome of HS- or HF-fed mice and fed standard facility chow in separate isolators. After 3 days of colonization, mice were started on 3% DSS ad libitum and weights were measured daily. Water supplemented with SCFA contained sodium acetate (0.554 g/100 mL), sodium butyrate (0.441 g/mL), and sodium propionate (0.249 g/mL), and sugar-supplemented water contained 10% sucrose, glucose, or fructose by weight. Tributyrin was added to high-sugar food (5% by weight) and glycerol was added to high-sugar and high-fiber food (5% by weight) as controls.

### Luminal Fluorescent Glucose Tracing

Mice were fasted for 8 hours and then anesthetized and a murine colonoscope (Storz) was inserted to remove luminal fecal contents and mucus (200  $\mu$ L PBS rinse). After 30 minutes, mice were anesthetized again to introduce 100  $\mu$ L Cy5-labeled glucose (synthesized by direct amide coupling of cyan fluorophores to 1-amino-1-deoxy-D-glucose, 100  $\mu$ mol/L diluted in PBS) or Cy5 secondary goat anti-rat antibody (100  $\mu$ mol/L diluted in PBS, A10525; ThermoFisher) into the colon via a gavage needle enema. Mice were supported inverted for 1 minute after the enema to ensure the probe remained in the colon and were taken down 30 minutes after for distal colon collection, fixed in 2% PFA (paraformaldehyde), and dehydrated in 30% sucrose overnight.

### Seahorse Metabolic Flux Analysis

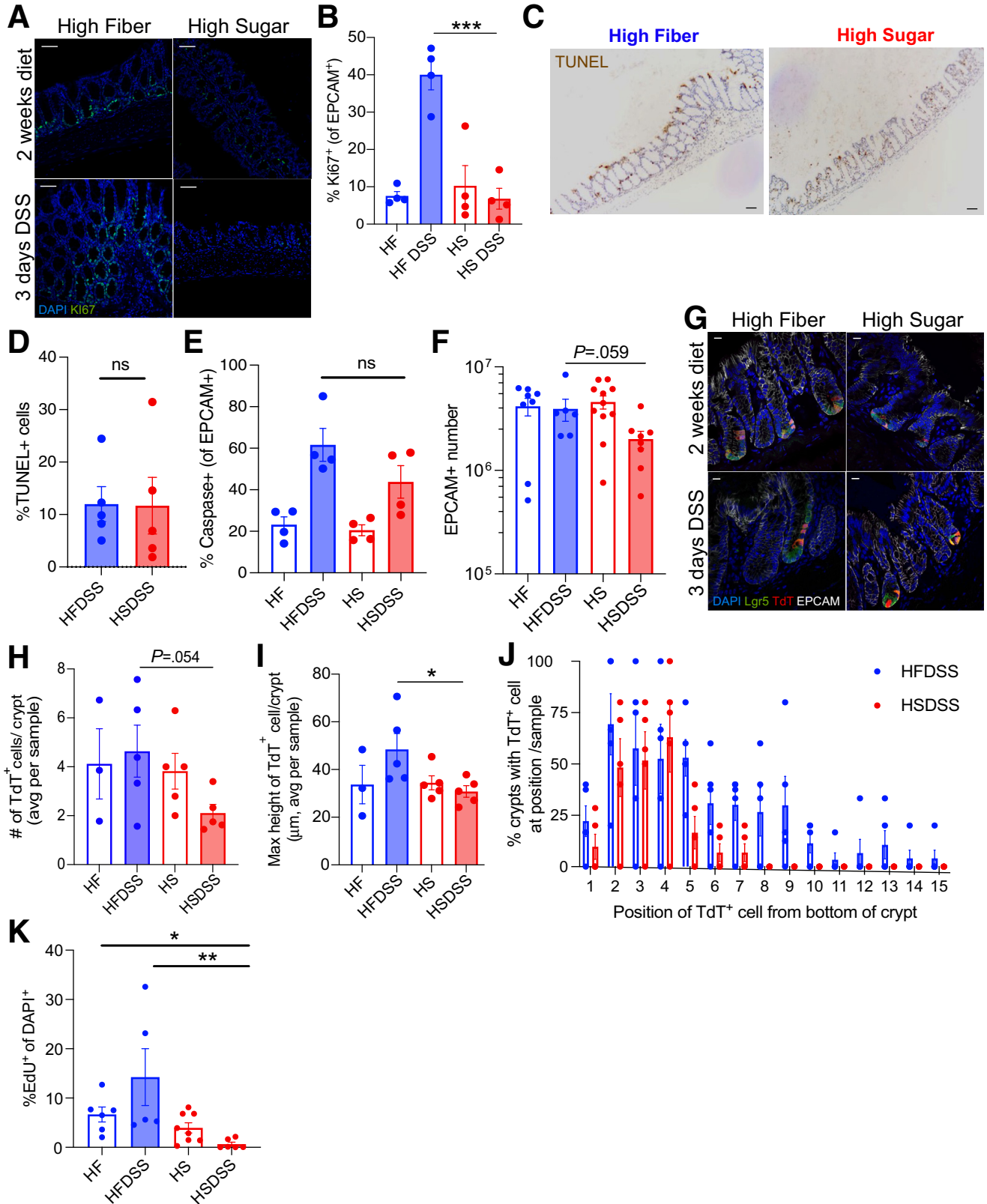
Crypts were isolated as described previously.<sup>14</sup> Crypts were seeded at 150 crypts/50  $\mu$ L on Cell-Tak-coated Seahorse Bioanalyzer XFe96 culture plates (Agilent, 300,000 or 100,000 cells/well, respectively) in assay media consisting of minimal, unbuffered DMEM supplemented with 1% BSA and 25 mmol/L glucose, 2 mmol/L glutamine, 1 mmol/L sodium pyruvate, and Matrigel. For colonic *Lgr5<sup>+</sup>* ISCs, cells were isolated from *Lgr5<sup>eGFP-IRES-Cre-ERT2</sup>* reporter mice fed defined diets for 2 weeks, as described previously,<sup>14</sup> and sorted into assay media with the addition of EGF (50 ng/mL), LDN-193189 (0.2  $\mu$ mol/L), R-spondin (500 ng/mL), N2 supplement (1 $\times$ ), B27 supplement (1 $\times$ ), Y-27632 (10

**Figure 14.** (See previous page). The transcriptome of the colonic epithelium with increased dietary sucrose at steady-state and after DSS-induced damage. (A and B) *Rag1<sup>-/-</sup>* mice were fed HF or HS diet for 2 weeks, and then exposed to 3% DSS drinking water for 7 days. (A) Percentage age initial weight and (B) survival shown (n = 3–4, means  $\pm$  SEM). (C–H) Bulk colonic epithelium was isolated from *Rag1<sup>-/-</sup>* female mice fed HS or HF diet for 2 weeks with or without 3 days of 3% DSS treatment and the transcriptome was measured via RNAseq (n = 3–4). (C) Expression level of epithelial subset gene signatures. (D) Principal Component Analysis (PCA) plot showing variance between samples from differentially treated mice (as indicated) with percentages on axes representing percentage variance explained by each principle component. (E) Volcano plot comparing genes isolated from colon epithelium of HS- or HF-treated mice and (F) volcano plot comparing genes isolated from colon epithelium of HS/DSS- or HF/DSS-treated mice. Red points represent differentially expressed genes ( $-1.5 > FC > 1.5$ ,  $*P < .05$ , FDR  $< 0.3$ ). Specific genes are called out with arrowheads. (G) GSEA of colonic epithelium RNAseq data showing enrichment of genes in HF/DSS-treated or HS/DSS-treated mice for gene sets as indicated. (H) Heatmap of regulatory enzymes of glycolysis and TCA cycle where red and blue represent high or low expression level, respectively, normalized across rows. For heatmaps, differentially expressed genes are denoted with a dagger, comparing HS/DSS vs HF/DSS epithelium ( $-1.5 > FC > 1.5$ ,  $*P < .05$ , FDR  $< 0.3$ ). Epi-Mes, Epithelial-Mesenchymal; max, maximum; min, minimum; Reg., regulatory.



$\mu\text{mol/L}$ ), and butyrate (5 mmol/L). Basal rates were taken for 30 minutes, and, in some experiments, oligomycin (2  $\mu\text{mol/L}$ ), FCCP (0.5  $\mu\text{mol/L}$  for crypts and 1.25  $\mu\text{mol/L}$  for

ISCs), 2-deoxy-d-glucose (10 mmol/L), and rotenone/anti-mycin A (0.5  $\mu\text{mol/L}$ ) were injected to obtain maximal respiratory and control values. SRC was measured as the



difference between the basal OCR and the maximum OCR after FCCP injection. A glucose stress test was used to determine the glycolytic response of crypts, in which crypts were placed in glucose-free media for 3 hours before adding exogenous glucose and ECAR values were measured while oligomycin (2  $\mu\text{mol/L}$ ), 2-deoxy-d-glucose (10  $\text{mmol/L}$ ), and rotenone/antimycin A (0.5  $\mu\text{mol/L}$ ) were injected into wells. Figures 11A, C, F, and H and Figures 12A and C show a representative trace of 1 experiment per cell type and combined data for SRC and the glycolytic rate (calculated as the difference between maximal ECAR after glucose injection and basal ECAR after 2-deoxyglucose injection).

### Blood Glucose Assay

Mice were fed defined diets for 2 weeks and then either fasted or allowed to eat overnight and blood was taken from the retro-orbital sinus after anesthesia with isoflurane. Glucose levels were measured using a Precision Xtra glucometer.

### Fluorescein Isothiocyanate–Dextran Assay

To evaluate gut permeability, 4 kilodalton fluorescein isothiocyanate (FITC)-dextran (Sigma-Aldrich) was dissolved in PBS (100  $\text{mg/mL}$ ) and mice were orally gavaged at 44  $\text{mg}/100 \text{ g}$  body weight after fasting for 8 hours. Mice were killed and blood was collected immediately via cardiac puncture. Serum was isolated and diluted with an equal volume of PBS, of which 100  $\mu\text{L}$  was added to a 96-well microplate in duplicate. The plate was read at an excitation of 485  $\text{nm}$  and an emission wavelength of 528  $\text{nm}$  to quantify FITC in blood, using serial dilutions of FITC-dextran to calculation concentration. Mice treated with DSS on standard diet and gavaged with FITC-dextran were used as a positive control of mice with a damaged intestinal barrier.

### Histologic Analysis of Colonic Tissue

Distal colon samples were fixed in formalin, dehydrated, and paraffin-embedded. Sections were stained with H&E stains for morphologic analysis and by TUNEL staining for apoptotic cell detection. Histopathology analysis was

blinded and determined using the following scoring criteria: (1) degree of inflammation in lamina propria (score, 0–3); (2) loss of goblet cells (score, 0–2); (3) abnormal crypts or epithelial hyperplasia with nuclear changes (score, 0–3); (4) presence of crypt abscesses (score, 0–3); (5) mucosal erosion and ulceration (score, 0–1); (6) submucosal spread to transmural involvement (score, 0–3); and (7) number of neutrophils (score, 0–4). Scores for the 7 parameters were combined for a total maximum score of 17.<sup>59</sup> Quantification of TUNEL was measured using ImageJ (National Institutes of Health) software analysis.

### 16s rRNA Gene Analysis of Bacterial Abundance in Intestine

Fecal samples were collected on the first day mice were started on their diets (initial), 2 weeks after starting their diets (standard or defined diets), and during DSS treatment (DSS) for SPF mice. DNA was isolated using the MoBio Power Soil Isolation Kit and polymerase chain reaction amplified at the V4 region of the 16S rRNA gene (515F-806R) and sequenced at the Argonne National Laboratory (Lemont, IL) on an Illumina MiSeq instrument. Microbiome informatics were performed using QIIME2 (Quantitative Insights Into Microbial Ecology 2) 2020.2.<sup>60</sup> Raw sequences were quality-filtered and denoised with DADA2.<sup>61</sup> Amplicon variant sequences were aligned with mafft and used to construct a phylogeny with fasttree2.<sup>62,63</sup> Alpha diversity metrics (observed Operational taxonomic unit, OTUs), beta diversity metrics (Bray Curtis dissimilarity), and principle coordinate analysis were estimated after samples were rarefied to 63,000 (subsampling without replacement) sequences per samples. Taxonomy was assigned to amplicon variant sequences using naive Bayes taxonomy classifier against the Greengenes 18.8 99% OTUs reference sequences.<sup>64</sup> All plots were made with publicly available R packages.

### Microscopy

Distal colonic tissue was flushed of luminal contents using PBS and fixed for 1 hour in 2% PFA (paraformaldehyde), dehydrated in 30% sucrose overnight at

**Figure 15.** (See previous page). After DSS-induced damage, HS diet reduces colonic crypt cell proliferation but does not increase epithelial cell death. (A and B) Colons were isolated from HS- or HF-fed mice, treated 3 days with or without DSS. (A) Representative images of colonic sections stained for Ki67 in green (magnification, 20 $\times$ ; scale bars: 50  $\mu\text{m}$ ) and (B) percentage of EPCAM<sup>+</sup> cells that are Ki67<sup>+</sup> from flow cytometric analysis. (C) Representative TUNEL of colonic sections after 3 days of 3% DSS treatment in mice fed HS or HF diet for 2 weeks. Images were taken at a magnification of  $\times 10$  (scale bars: 100  $\mu\text{m}$ ). (D) Percentage of cells that are TUNEL<sup>+</sup>. (E) Mice were fed HS or HF diet and treated 3 days with 3% DSS, colonic epithelium was isolated and stained with activated caspase-3 for flow cytometric analysis. Data represent the percentage of EPCAM<sup>+</sup> cells that are activated caspase-3<sup>+</sup>. (F) Number of EPCAM<sup>+</sup> colonocytes after 4 days of DSS from flow cytometric analysis. (G–J) *Lgr5*<sup>eGFP-Cre-ERT2</sup> *Rosa*<sup>LSL-TandemDimerTomato</sup> mice fed HS or HF diet for 2 weeks and injected with tamoxifen to induce Tomato expression from *Lgr5*-expressing ISCs on first day of DSS treatment. (G) Representative images of colonic crypts with *Lgr5*<sup>eGFP</sup> (green) and Tomato<sup>+</sup> progeny (red) (magnification, 60 $\times$ ; scale bars: 10  $\mu\text{m}$ ), (H) number of TdT<sup>+</sup> cells per crypt, (I) height of most distant Tomato<sup>+</sup> progeny from bottom of crypt (averaged per GFP<sup>+</sup> crypt), and (J) percentage of GFP<sup>+</sup> crypts containing Tomato<sup>+</sup> progeny at the specified position along crypts are shown after 3 days of DSS. (K) *Lgr5*<sup>eGFP-Cre-ERT2</sup> *Rosa*<sup>LSL-TdTomato</sup> mice were fed HS or HF diet for 2 weeks, injected with tamoxifen to induce Tomato expression on the first day of DSS treatment, and injected with EdU on day 3 of DSS, 4 hours before being killed. Percentage of EdU<sup>+</sup> cells, as measured by microscopy, are shown. Data are representative of 2 experiments ( $n = 2-5$ ) and data points represent means  $\pm$  SEM. (F and K) One-way analysis of variance or Kruskal–Wallis test were used to determine significance, where \* $P < .05$ , \*\* $P < .01$ , and \*\*\* $P < .001$ . avg, average; DAPI, 4',6-diamidino-2-phenylindole; Max, maximum.

**Table 1.** Dietary Composition of Standard and Defined Diets

Ingredient	Standard	High fiber	High sugar
Protein	26.1% kcal	17.8% kcal	17.8% kcal
Casein	<sup>a</sup>	155.5 g/kg	200.0 g/kg
Methionine	5.8 g/kg	3.0 g/kg	3.0 g/kg
Carbohydrate	59.6% kcal	70.5% kcal	70.5% kcal
Sucrose	14.1 g/kg	22.0 g/kg	663.5 g/kg
High-amylose corn starch	313 g/kg	699.0 g/kg	2.0 g/kg
Maltodextrin	0 g/kg	20.0 g/kg	20.0 g/kg
Cellulose	208 g/kg	9.89 g/kg	9.89 g/kg
Fat	14.3%	11.7% kcal	11.7% kcal
Soybean	<sup>a</sup>	39.0 g/kg	50.0 g/kg
Vitamin mix	<sup>a</sup>	10.0 g/kg	10.0 g/kg
Choline bitartrate	<sup>a</sup>	2.5 g/kg	2.5 g/kg
TBHQ, antioxidant	<sup>a</sup>	0.01 g/kg	0.01 g/kg
Mineral mix	<sup>a</sup>	35.0 g/kg	35.0 g/kg
Calcium phosphate, dibasic	<sup>a</sup>	4.0 g/kg	4.0 g/kg

NOTE. High-fiber and high-sugar diets were designed to have the same macronutrient composition (the percentage of calories coming from protein, carbohydrates, and fat were kept constant) with identical ingredients. Units indicate grams of ingredient per kilogram of food.

TBHQ, tert-butylhydroquinone.

<sup>a</sup>Different ingredients were used in the standard diet (Prolab IsoPro RMH 3000, 5P75).

4°C, and flash-frozen in OTC (organotypic 3D culture) media. Sections were stained with antibodies specific to EPCAM (clone G8.8, catalog #118212; BioLegend), phospho-PDH (Ser 293, ref 31866; Cell Signaling), and Ki67 (clone SolA15, ref 14-5698-82; Invitrogen) overnight, and for 5 minutes for the Hoechst nuclear stain (ref H3570; Invitrogen). For EdU identification, slides were permeabilized with Triton-X-100 (Dow) for 10 minutes and stained in Click-It cocktail (ThermoFisher) for 20 minutes at room temperature. Images were taken on Zeiss LSM 510 and Nikon A1 confocal microscopes and analyzed using ImageJ software.

### Flow Cytometry

All antibodies used for flow cytometry were purchased from either ThermoFisher, BD Biosciences, or BioLegend. The antibodies we used for flow cytometry were as follows: CD45.2 (clone 104, ref 47-0454-82; Invitrogen), EPCAM (clone G8.8, catalog #563478; BD Biosciences), activated caspase-3 (clone C92-605, catalog #560901; BD Biosciences), Ki67 (clone 16A8, catalog #652403; BioLegend), MitoTracker Deep Red (catalog #M22426; ThermoFisher), and MitoSox (catalog #M36008; ThermoFisher). Dead cells were discriminated in all experiments using live/dead fixable dead stain (catalog #501121526; ThermoFisher). All stains were performed in media containing anti-CD16/32 blocking antibody (clone 93, catalog #14-0161-86; ThermoFisher). All flow cytometry was acquired on an LSRFortessa FACS analyzer (Becton, Dickinson and Company (BD) San Diego, CA). Cells were isolated from the colon for flow cytometry using EDTA and dithiothreitol dissociation and shaking to release the epithelium from the lamina propria.<sup>65</sup> To separate intraepithelial cells, the cell suspension was

spun down in a 30% Percoll gradient. Analysis of flow cytometry was performed using FlowJo software (TreeStar).

### Tamoxifen and EdU Administration

Tamoxifen (Sigma-Aldrich) was orally gavaged at 5 mg/mouse per day on the first day of DSS treatment. Because tamoxifen is poorly soluble in water, the amount needed for a single day was dissolved in 95% ethanol, heating to 37°C, and diluted in corn oil (Sigma) such that 100 µL had 5 mg. EdU (5 mg) was injected intraperitoneally in mice (in 200 µL PBS) 4 hours before being killed on the third day of 3% DSS treatment.

### Statistical Analysis

Statistical tests are as indicated in the figure legends. Lines in scatter plots represent the means for the group. Group sizes were determined based on the results of preliminary experiments. Mouse studies were performed in a nonblinded manner. All statistical analyses were calculated using Prism software (GraphPad). Differences were considered statistically significant when  $P < .05$ .

### References

1. Barker N, Es JH van, Kuipers J, et al. Identification of stem cells in small intestine and colon by marker gene *Lgr5*. *Nature* 2007;449:1003–1007.
2. Bjerknes M, Cheng H. Clonal analysis of mouse intestinal epithelial progenitors. *Gastroenterology* 1999; 116:7–14.
3. Cheng H, Leblond CP. Origin, differentiation and renewal of the four main epithelial cell types in the mouse small intestine. V. Unitarian theory of the origin of the four epithelial cell types. *Am J Anat* 1974;141:537–561.

4. Potten CS. A comprehensive study of the radiobiological response of the murine (BDF1) small intestine. *Int J Radiat Biol* 1990;58:925–973.
5. Beyaz S, Mana MD, Roper J, et al. High-fat diet enhances stemness and tumorigenicity of intestinal progenitors. *Nature* 2016;531:53–58.
6. Fan Y-Y, Davidson LA, Callaway ES, et al. A bioassay to measure energy metabolism in mouse colonic crypts, organoids, and sorted stem cells. *Am J Physiol Gastrointest Liver Physiol* 2015;309:G1–G9.
7. Monteiro CA, Moubarac JC, Cannon G, et al. Ultra-processed products are becoming dominant in the global food system. *Obes Rev* 2013;14(Suppl 2):21–28.
8. Spreadbury I. Comparison with ancestral diets suggests dense acellular carbohydrates promote an inflammatory microbiota, and may be the primary dietary cause of leptin resistance and obesity. *Diabetes Metab Syndr Obes* 2012;5:175–189.
9. Grundy MM-L, Edwards CH, Mackie AR, et al. Re-evaluation of the mechanisms of dietary fibre and implications for macronutrient bioaccessibility, digestion and postprandial metabolism. *Br J Nutr* 2016;116:816–833.
10. Kearney J. Food consumption trends and drivers. *Philos Trans R Soc Lond B Biol Sci* 2010;365:2793–2807.
11. Palmer CS, Ostrowski M, Balderson B, et al. Glucose metabolism regulates T cell activation, differentiation, and functions. *Front Immunol* 2015;6:1.
12. Chen L, Vasoya RP, Toke NH, et al. HNF4 regulates fatty acid oxidation and is required for renewal of intestinal stem cells in mice. *Gastroenterology* 2020;158:985–999.e9.
13. Mihaylova MM, Cheng C-W, Cao AQ, et al. Fasting activates fatty acid oxidation to enhance intestinal stem cell function during homeostasis and aging. *Cell Stem Cell* 2018;22:769–778.e4.
14. Stine RR, Sakers AP, TeSlaa T, et al. PRDM16 maintains homeostasis of the intestinal epithelium by controlling region-specific metabolism. *Cell Stem Cell* 2019;25:830–845.e8.
15. Kerbey AL, Randle PJ, Cooper RH, et al. Regulation of pyruvate dehydrogenase in rat heart. Mechanism of regulation of proportions of dephosphorylated and phosphorylated enzyme by oxidation of fatty acids and ketone bodies and of effects of diabetes: role of coenzyme A, acetyl-coenzyme A and reduced and oxidized nicotinamide-adenine dinucleotide. *Biochem J* 1976;154:327–348.
16. Michelakis ED, Sutendra G, Dromparis P, et al. Metabolic modulation of glioblastoma with dichloroacetate. *Sci Transl Med* 2010;2:31ra34.
17. Xu H, Liu X, Yang J, et al. Cyanine-based 1-amino-1-deoxyglucose as fluorescent probes for glucose transporter mediated bioimaging. *Biochem Biophys Res Commun* 2016;474:240–246.
18. Watson MJ, Vignali PDA, Mullett SJ, et al. Metabolic support of tumour-infiltrating regulatory T cells by lactic acid. *Nature* 2021;591:645–651.
19. Sinclair LV, Barthelemy C, Cantrell DA. Single cell glucose uptake assays: a cautionary tale. *Immunometabolism* 2020;2:e200029.
20. Yoshikawa T, Inoue R, Matsumoto M, et al. Comparative expression of hexose transporters (SGLT1, GLUT1, GLUT2 and GLUT5) throughout the mouse gastrointestinal tract. *Histochem Cell Biol* 2011;135:183–194.
21. Röder PV, Geillinger KE, Zietek TS, et al. The role of SGLT1 and GLUT2 in intestinal glucose transport and sensing. *PLoS One* 2014;9:e89977.
22. Wang Y, Song W, Wang J, et al. Single-cell transcriptome analysis reveals differential nutrient absorption functions in human intestine. *J Exp Med* 2020;217:e20191130.
23. Thaiss CA, Levy M, Grosheva I, et al. Hyperglycemia drives intestinal barrier dysfunction and risk for enteric infection. *Science* 2018;359:1376–1383.
24. Sciafani A, Zukerman S, Ackroff K. Fructose- and glucose-conditioned preferences in FVB mice: strain differences in post-oral sugar appetite. *Am J Physiol Regul Integr Comp Physiol* 2014;307:R1448–R1457.
25. Nunes NS, Kim S, Sundby M, et al. Temporal clinical, proteomic, histological and cellular immune responses of dextran sulfate sodium-induced acute colitis. *World J Gastroenterol* 2018;24:4341–4355.
26. Ayres JS, Trinidad NJ, Vance RE. Lethal inflammasome activation by a multidrug-resistant pathobiont upon antibiotic disruption of the microbiota. *Nat Med* 2012;18:799–806.
27. Kamada N, Chen GY, Inohara N, et al. Control of pathogens and pathobionts by the gut microbiota. *Nat Immunol* 2013;14:685–690.
28. Lupp C, Robertson ML, Wickham ME, et al. Host-mediated inflammation disrupts the intestinal microbiota and promotes the overgrowth of Enterobacteriaceae. *Cell Host Microbe* 2007;2:119–129.
29. Khan S, Waliullah S, Godfrey V, et al. Dietary simple sugars alter microbial ecology in the gut and promote colitis in mice. *Sci Transl Med* 2020;12:eaay6218.
30. Desai MS, Seekatz AM, Koropatkin NM, et al. A dietary fiber-deprived gut microbiota degrades the colonic mucus barrier and enhances pathogen susceptibility. *Cell* 2016;167:1339–1353.e21.
31. Kelly CJ, Zheng L, Campbell EL, et al. Crosstalk between microbiota-derived short-chain fatty acids and intestinal epithelial HIF augments tissue barrier function. *Cell Host Microbe* 2015;17:662–671.
32. Wong JMW, Souza R de, Kendall CWC, et al. Colonic health: fermentation and short chain fatty acids. *J Clin Gastroenterol* 2006;40:235–243.
33. Furusawa Y, Obata Y, Fukuda S, et al. Commensal microbe-derived butyrate induces the differentiation of colonic regulatory T cells. *Nature* 2013;504:446–450.
34. Byndloss MX, Olsan EE, Rivera-Chávez F, et al. Microbiota-activated PPAR- $\gamma$  signaling inhibits dysbiotic Enterobacteriaceae expansion. *Science* 2017;357:570–575.
35. Desler C, Hansen TL, Frederiksen JB, et al. Is there a link between mitochondrial reserve respiratory capacity and aging? *J Aging Res* 2012;2012:192503.

36. Zhou Y, Al-Saaidi RA, Fernandez-Guerra P, et al. Mitochondrial spare respiratory capacity is negatively correlated with nuclear reprogramming efficiency. *Stem Cells Dev* 2017;26:166–176.
37. Varum S, Momcilović O, Castro C, et al. Enhancement of human embryonic stem cell pluripotency through inhibition of the mitochondrial respiratory chain. *Stem Cell Res* 2009;3:142–156.
38. Traba J, Miozzo P, Akkaya B, et al. An optimized protocol to analyze glycolysis and mitochondrial respiration in lymphocytes. *J Vis Exp* 2016;117:54918.
39. Scharl M, Huber N, Lang S, et al. Hallmarks of epithelial to mesenchymal transition are detectable in Crohn's disease associated intestinal fibrosis. *Clin Transl Med* 2015;4:1.
40. Harnack C, Berger H, Antanaviciute A, et al. R-spondin 3 promotes stem cell recovery and epithelial regeneration in the colon. *Nat Commun* 2019;10:4368.
41. Sato T, Es JH van, Snippert HJ, et al. Paneth cells constitute the niche for Lgr5 stem cells in intestinal crypts. *Nature* 2011;469:415–418.
42. Rodríguez-Colman MJ, Schewe M, Meerlo M, et al. Interplay between metabolic identities in the intestinal crypt supports stem cell function. *Nature* 2017;543:424–427.
43. Bensard CL, Wisidagama DR, Olson KA, et al. Regulation of tumor initiation by the mitochondrial pyruvate carrier. *Cell Metab* 2020;31:284–300.e7.
44. Sidossis LS, Wolfe RR. Glucose and insulin-induced inhibition of fatty acid oxidation: the glucose-fatty acid cycle reversed. *Am J Physiol* 1996;270:E733–E738.
45. Visiedo F, Bugatto F, Sánchez V, et al. High glucose levels reduce fatty acid oxidation and increase triglyceride accumulation in human placenta. *Am J Physiol Endocrinol Metab* 2013;305:E205–E212.
46. Tataranni T, Piccoli C. Dichloroacetate (DCA) and cancer: an overview towards clinical applications. *Oxid Med Cell Longev* 2019;2019:8201079.
47. Carey BW, Finley LWS, Cross JR, et al. Intracellular  $\alpha$ -ketoglutarate maintains the pluripotency of embryonic stem cells. *Nature* 2015;518:413–416.
48. Racine A, Carbonnel F, Chan SSM, et al. Dietary patterns and risk of inflammatory bowel disease in Europe: results from the EPIC study. *Inflamm Bowel Dis* 2016;22:345–354.
49. Hou JK, Abraham B, El-Serag H. Dietary intake and risk of developing inflammatory bowel disease: a systematic review of the literature. *Am J Gastroenterol* 2011;106:563–573.
50. Miyoshi H, Stappenbeck TS. In vitro expansion and genetic modification of gastrointestinal stem cells in spheroid culture. *Nat Protoc* 2013;8:2471–2482.
51. Mackay GM, Zheng L, van den Broek NJF, et al. Analysis of cell metabolism using LC-MS and isotope tracers. *Meth Enzymol* 2015;561:171–196.
52. Trapnell C, Roberts A, Goff L, et al. Differential gene and transcript expression analysis of RNA-seq experiments with TopHat and Cufflinks. *Nat Protoc* 2012;7:562–578.
53. Obih C, Wahbeh G, Lee D, et al. Specific carbohydrate diet for pediatric inflammatory bowel disease in clinical practice within an academic IBD center. *Nutrition* 2016;32:418–425.
54. Yeh A, Conners EM, Ramos-Jimenez RG, et al. Plant-based enteral nutrition modifies the gut microbiota and improves outcomes in murine models of colitis. *Cell Mol Gastroenterol Hepatol* 2019;7:872–874.e6.
55. Laffin M, Fedorak R, Zalasky A, et al. A high-sugar diet rapidly enhances susceptibility to colitis via depletion of luminal short-chain fatty acids in mice. *Sci Rep* 2019;9:12294.
56. Koretz RL, Lipman TO, Klein S, et al. AGA technical review on parenteral nutrition. *Gastroenterology* 2001;121:970–1001.
57. Grover Z, Muir R, Lewindon P. Exclusive enteral nutrition induces early clinical, mucosal and transmural remission in paediatric Crohn's disease. *J Gastroenterol* 2014;49:638–645.
58. Bolger AM, Lohse M, Usadel B. Trimmomatic: a flexible trimmer for Illumina sequence data. *Bioinformatics* 2014;30:2114–2120.
59. Ostanin DV, Bao J, Koboziev I, et al. T cell transfer model of chronic colitis: concepts, considerations, and tricks of the trade. *Am J Physiol Gastrointest Liver Physiol* 2009;296:G135–G146.
60. Bolyen E, Rideout JR, Dillon MR, et al. Reproducible, interactive, scalable and extensible microbiome data science using QIIME 2. *Nat Biotechnol* 2019;37:852–857.
61. Callahan BJ, McMurdie PJ, Rosen MJ, et al. DADA2: high-resolution sample inference from Illumina amplicon data. *Nat Methods* 2016;13:581–583.
62. Katoh K, Misawa K, Kuma K, et al. MAFFT: a novel method for rapid multiple sequence alignment based on fast Fourier transform. *Nucleic Acids Res* 2002;30:3059–3066.
63. Price MN, Dehal PS, Arkin AP. FastTree 2—approximately maximum-likelihood trees for large alignments. *PLoS One* 2010;5:e9490.
64. McDonald D, Price MN, Goodrich J, et al. An improved Greengenes taxonomy with explicit ranks for ecological and evolutionary analyses of bacteria and archaea. *ISME J* 2012;6:610–618.
65. Hall JA, Cannons JL, Grainger JR, et al. Essential role for retinoic acid in the promotion of CD4(+) T cell effector responses via retinoic acid receptor alpha. *Immunity* 2011;34:435–447.

---

Received October 27, 2022. Accepted May 4, 2023.

#### Correspondence

Address correspondence to: Timothy W. Hand, PhD, Department of Pediatrics, University of Pittsburgh, 4401 Penn Avenue, Rangos Research Building 8126, Pittsburgh, Pennsylvania 15224. e-mail: [timothy.hand@chp.edu](mailto:timothy.hand@chp.edu).

#### Acknowledgments

The authors would like to thank M. Meyers and S. Reynolds from University of Pittsburgh Medical Center (UPMC) Hillman Institute of Cancer flow core for cell sorting; J. Toothaker for assistance in image analysis; A.S. Costa, E. Kilic, and J. Cross for assistance with the metabolomics analysis; J. Deschepper and the University of Pittsburgh Gnotobiotic Animal Core for gnotobiotic experiments; the staff of the Division of Laboratory Animal Services for animal husbandry; the UPMC Children's Hospital of Pittsburgh Histology Core; W. MacDonald and R. Elbakri at the University of Pittsburgh Health Science Sequencing Core; S. Watkins and the Center for Biological Imaging; the University of Pittsburgh Center for Research Computing; and the members of the Hand, Beyaz, Delgoffe, Cooper, and Poholek laboratories for helpful discussions.

**CRedit Authorship Contributions**

Ansen H.P. Burr, BS (Conceptualization: Equal; Formal analysis: Lead; Funding acquisition: Supporting; Investigation: Equal; Methodology: Equal; Validation: Equal; Writing – original draft: Equal; Writing – review & editing: Equal)

Junyi Ji, BMED (Conceptualization: Equal; Formal analysis: Equal; Investigation: Equal)

Kadir Ozler, BS (Investigation: Equal)

Heather L Mentrup, PhD (Investigation: Supporting; Methodology: Supporting)

Onur Eskiocak, BS (Investigation: Supporting)

Brian Yueh, BS (Investigation: Supporting)

Rachel Cumberland, BA (Investigation: Supporting; Methodology: Supporting)

Ashley V Menk, BS (Formal analysis: Supporting; Investigation: Equal)

Natalie Rittenhouse, BS (Formal analysis: Supporting)

Chris W Marshall, PHD (Formal analysis: Supporting)

Pailin Chiaranunt, BS (Investigation: Supporting)

Xiaoyi Zhang, MD/PhD (Investigation: Supporting), Lauren Mullinax, MD (Investigation: Supporting)

Abigail Overacre-Delgoffe, PhD (Formal analysis: Supporting; Funding acquisition: Supporting)

Vaughn S. Cooper, PhD (Formal analysis: Supporting), Amanda C. Poholek, PhD (Formal analysis: Supporting)

Greg M. Delgoffe, PhD (Formal analysis: Supporting; Resources: Supporting; Writing – review & editing: Supporting)

Kevin P Mollen, MD (Conceptualization: Supporting; Resources: Supporting)

Semir Beyaz, PhD (Conceptualization: Supporting; Formal analysis: Equal; Resources: Equal; Writing – review & editing: Supporting)

Timothy W. Hand, PhD (Conceptualization: Equal; Funding acquisition: Lead; Resources: Lead; Supervision: Lead; Writing – review & editing: Equal)

**Conflicts of interest**

The authors disclose no conflicts.

**Funding**

This work was supported by the Richard King Mellon Institute for Pediatric Research, National Institutes of Health grant T32AI089443-10 (A.H.P.B.), Damon Runyon Cancer Research Foundation Postdoctoral Fellowship grant 2360-19 (A.O.D.), and the Kenneth Rainin Foundation (Innovator's Award). This work was performed with assistance from the Cold Spring Harbor Laboratories Mass Spectrometry Shared Resource, which is supported by the Cancer Center Support grant 5P30CA045508.

**Data Availability**

All relevant data, associated protocols, and materials are present in this manuscript. Original sequencing data sets can be found at the NCBI repository upon publication. Accession numbers: 16S rRNA amplicon microbiota sequencing (PRJNA690134), in vivo epithelium RNAseq (PRJNA971990), Lgr5 cell RNAseq (PRJNA972287), and mouse colonoid RNAseq. (PRJNA972422).